TÜBİTAK

Turkish Journal of Earth Sciences

http://journals.tubitak.gov.tr/earth/

Research Article

Turkish J Earth Sci
(2021) 30: 1112-1133

doi:10.3906/yer-2105-15

Hydrogeochemical and isotopic monitoring of the Kestanbol geothermal field (Northwestern Turkey) and its relationship with seismic activity

Deniz ŞANLIYÜKSEL YÜCEL[1,*], Süha ÖZDEN[2], Harika MARMARA[3]

[1]Department of Mining Engineering, Faculty of Engineering, Çanakkale Onsekiz Mart University, Çanakkale, Turkey
[2]Department of Geological Engineering, Faculty of Engineering, Çanakkale Onsekiz Mart University, Çanakkale, Turkey
[3]Department of Geological Engineering, School of Graduate Studies, Çanakkale Onsekiz Mart University, Çanakkale, Turkey

Received: 08.05.2021 • **Accepted/Published Online:** 30.09.2021 • **Final Version:** 01.12.2021

Abstract: Kestanbol geothermal field is located in northwestern Turkey and is one of the highest temperature geothermal fields in the Biga Peninsula. In this study, one geothermal well, two geothermal springs, and two cold springs were monitored for one year in Kestanbol geothermal field to determine hydrogeochemical and isotopic characteristics. Additionally, any possible relationship between seismic activity and variations in the hydrochemistry of geothermal water was investigated. The Kestanbol geothermal field is controlled mainly by the right-lateral strike-slip Kaplıca fault with normal components. The distribution of the geothermal waters is roughly parallel to the fault. The temperature, electrical conductivity, salinity, and pH value of the geothermal waters were within the range of 59.5 to 74.6 °C, 30300 to 35700 µS/cm, 19.6 to 23.3‰ and 6.13 to 6.83, respectively. The temperature interval was from 11.2 to 25.4 °C for cold waters. The hydrochemical facies of the geothermal waters were Na-Cl type, and the cold waters were Ca-HCO_3-Cl type. The high concentrations of As, Ba, Fe, Li, and Mn in geothermal waters were mainly derived from prolonged water-rock interactions under high-temperature conditions. The $\delta^{18}O$ and $\delta^{2}H$ contents of cold waters indicated meteoric origin. The geothermal waters were enriched in $\delta^{18}O$ and $\delta^{2}H$ and located on the mixing line between local groundwater and fossil seawater, indicating mixing processes. During our study period, 20 earthquakes with Mw 3.5 and above were recorded in the close surroundings of the Kestanbol geothermal field, and temporal variations in the physicochemical and chemical compositions of geothermal waters were observed. Concentrations Cl^- of the geothermal waters exhibited decrease after the Tartışık-Ayvacık earthquake (Mw = 5.0), indicating more supplement of groundwater with shallow origin under the increase of tectonic stress.

Key words: Kestanbol geothermal field, active tectonics, hydrogeochemistry, isotope, water-rock interaction, fossil seawater

1. Introduction

It has been documented for thousands of years that earthquakes and other tectonic processes cause temporary or permanent hydrogeochemical changes in cold and geothermal waters (King and Manga, 2018). In seismically active areas, continuous monitoring of the hydrochemistry of geothermal waters is an approach used to understand the mechanisms affecting earthquake occurrence and the response of the crust in the affected region (Suer et al., 2008). After earthquakes (Mw ≥ 5), changes were observed in 20 different parameters such as temperature and Na^+, Ca^{2+}, Mg^+, Cl^-, F^-, SO_4^{2-}, HCO_3^-, and trace element concentrations in groundwater (Tsunogai and Wakita, 1996; Claesson et al., 2004; Huang et al., 2004; Skelton et al., 2008; Du et al., 2010; Chen et al., 2014; Shi et al., 2015; Nakagawa et al., 2020). Tsunogai and Wakita (1996) collected 79 samples from groundwater after the Hyogo-ken Nanbu destructive earthquake (M = 7.2) occurring in southwestern Japan on January 17, 1995. They observed increases in Cl^- and SO_4^{2-} and reductions in Na^+ and Si, and stated that these changes might be due to mixing of shallow groundwater. Chen et al. (2014) investigated the effect of the Wenchuan earthquake (Ms = 8) occurring in Sichuan province in China on May 12, 2008 on hydrochemical characterization of 32 geothermal waters. They identified increases in K^+ and SO_4^{2-} in geothermal waters and attributed to the interfusion of the deep fluids by the increased tectonic stress.

As an important part of the Alpine-Himalayan orogenic belt, Turkey is characterized by numerous medium- and high-temperature geothermal fields (Mutlu and Gulec, 1998). The distribution of geothermal fields in Turkey is strongly consistent with the distribution of tectonic patterns and recent volcanic activity (Vengosh et al., 2002). Studies in Turkey identified more than 460 geothermal fields with over 2000 geothermal springs and wells with

* Correspondence: denizsyuksel@comu.edu.tr

temperatures varying from 20 to 287 °C (Mertoglu et al., 2020; Lund and Toth, 2021).

Detailed studies increased in order to determine the relationship between the hydrochemical changes in geothermal waters and the active tectonic regime in the last 20 years in Turkey. Simsek and Yildirim (2000) stated there were changes observed in the turbidity, odor, taste, color, temperature, pressure, flow, and chemical variations in some geothermal waters and cold waters before and after earthquakes on August 17, 1999 in Gölcük (Mw = 7.4) and November 12, 1999 in Düzce (Mw = 7.2). They observed turbidity and flow increases in Efteni geothermal water one day before the earthquake and these changes returned to normal one week later. Balderer et al. (2002) determined some short-term changes in physicochemical (temperature, pH, and electrical conductivity), chemical (Ca^{2+}, Na^{+}, K^{+}, Cl^{-} and SO_4^{2-}) parameters and isotopic (δ^2H and $\delta^{18}O$) characterization of geothermal waters in the Kuzuluk, Bursa and Yalova/Gemlik along the North Anatolian Fault Zone (NAFZ) after the Gölcük earthquake. They stated that these changes might be the result of induced groundwater circulation. Belin et al. (2002) investigated the changes in metal concentrations in 5 geothermal wells in the Kuzuluk geothermal field located on the NAFZ before and after the Gölcük and Düzce earthquakes. They showed that the Pb, Cr, Ni, and Cu concentrations increased, while Fe, Zn, Mn, Co and Cd concentrations decreased in geothermal water before and after the earthquakes. Suer et al. (2008) monitored chemical and isotopic characterization in the Yalova, Efteni, Bolu, Mudurnu, Seben, Kurşunlu, Çankırı, Hamamözü, Gözlek, and Reşadiye geothermal fields located along E-W transect of the NAFZ for possible relationships with seismic activity. They stated that Cl^{-}, Ca^{2+} and ^3H were the most sensitive tracers of seismically-induced crustal perturbations. The hydrochemical changes due to active tectonics were observed most clearly in the Yalova and Efteni geothermal fields. Yuce et al. (2010) researched earthquakes occurring on the Thrace-Eskişehir Fault Zone and effects on physical and chemical variations in geothermal waters from the Uyuzhamam and Hamamkarahisar geothermal fields. They emphasized that monitoring the Rn and CO_2 gas concentrations and water level changes in geothermal waters was more effective in identifying hydrochemical variations linked to shallow earthquakes. Ates and Tutkun (2014) researched the relationship between seismic activity and hydrochemical characteristics of geothermal waters in Çitgöl, Eynal and Naşa geothermal fields. They stated that increase in temperature and Cl^{-} and reduction in SO_4^{2-} occurred in geothermal waters after the earthquakes with a magnitude >5. Kacar et al. (2017) performed sampling in 12 different periods from 4 geothermal wells in the Güre geothermal field and assessed the hydrochemical analysis results with earthquakes with a magnitude >3 affecting geothermal field. They identified variations in pH value, temperature, electrical conductivity, Na^{+}, Cl^{-}, and SO_4^{2-} in geothermal water and associated these variations with the active tectonic regime in the region.

The Biga Peninsula located in northwest Turkey is affected by the NAFZ along with the Western Anatolian Graben System and is characterized by active fault systems from the Upper Miocene to the present day (Samilgil, 1966; Ozden et al., 2018). Yalcin and Sarp (2012) reported that there were 20 geothermal fields with surface temperatures from 31.5 to 104.4 °C located in the Biga Peninsula and that geothermal springs emerged from NE-SW striking right-lateral strike-slip fault systems. One of the highest temperature geothermal fields with in the Biga Peninsula is Kestanbol located about 50 km southwest of Çanakkale and in the Alexandria Troas ancient port city (Figure 1a). Strabo (64 BC-AD 24) mentioned that Alexandria Troas was an important Roman city, in addition to being popular for geothermal springs and baths (Leaf, 1923; Tasci, 1995). Demirsoy et al. (2018) stated that the Kestanbol geothermal springs were used for medical treatments and bathing since the Hellenistic period (330-30 BC). According to the report by Professor Gautier from the Paris Medical Academy in 1894, the Kestanbol geothermal springs were proven to be effective for treating different diseases like rheumatic diseases, calcification, bone tuberculosis, upper respiratory tract, and lung diseases (Demirsoy et al., 2017).

The Kestanbol geothermal field is about 3.3 km from the Aegean Sea, and it's located 30–40 m above sea level. The climate of Çanakkale is typified by warm, arid summers and mild, rainy winters. The long-term (1929-2020) mean total precipitation was 624 mm per year, based on data collected at the Çanakkale Meteorological Station. The temperature varied between –11.5 °C on February 9, 1929 and 39.1 °C on August 6, 2017, with a mean of 15.1 °C. A well was drilled in the aquifer in 1975 to a depth of 290.7 m by the General Directorate of Mineral Research and Exploration (MTA) to evaluate the geothermal potential of the Kestanbol geothermal field. The reservoir temperature and flow rate of geothermal water was identified as 75 °C and 25 L/s, respectively (Olmez, 1976). Nowadays, the geothermal well is utilized for thermal tourism and heating the spa located in the geothermal field.

Previous studies were performed to identify the geological, hydrogeological, and hydrogeochemical characterization of Kestanbol geothermal field and to use geoelectric methods for geothermal exploration, in addition to evaluating the environmental effects of Kestanbol geothermal water on soil and stream sediment (Olmez, 1976; Mutzenberg, 1997; Caglar and Demirorer, 1999; Baba and Ertekin, 2007; Tokcaer, 2007; Yalcin, 2007; Yalcin and Sarp, 2012; Karaca et al., 2013,

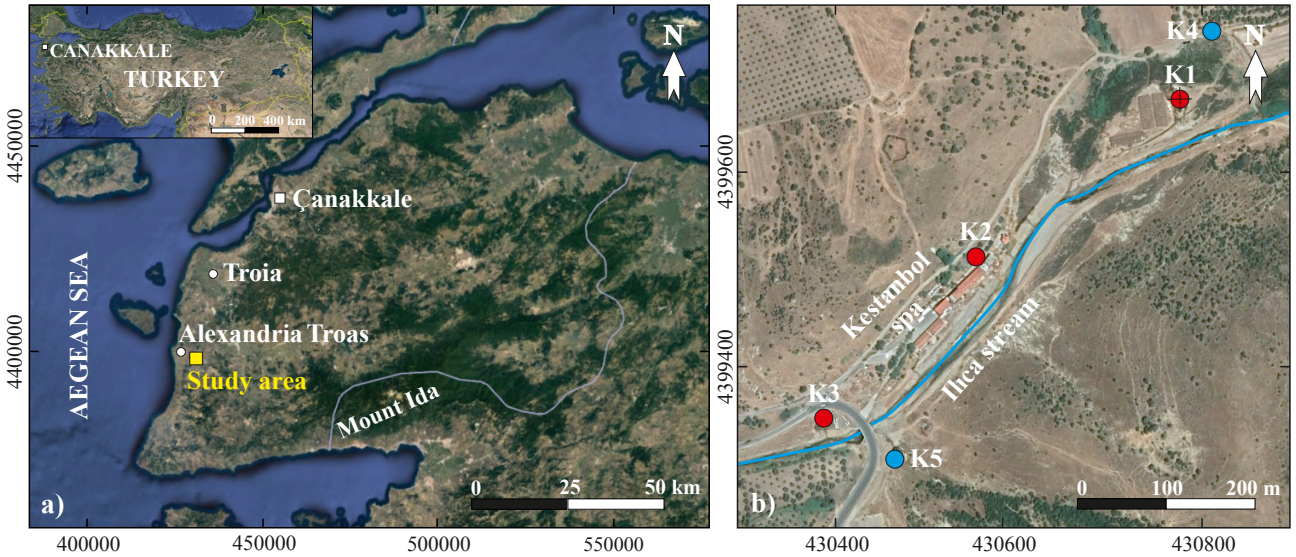

Figure 1. Location map of the a) Kestanbol geothermal field, b) water sampling points.

Marmara et al., 2020). This study aimed to (1) determine the hydrogeochemical and isotopic compositions of geothermal and cold waters in the Kestanbol geothermal field and (2) investigate the effect of seismic activity on variations in the hydrogeochemical features of the Kestanbol geothermal waters.

2. Materials and methods

2.1. Field studies

Water sampling was carried out at five points from one geothermal well (K1), two geothermal springs (K2 and K3), and two cold springs (K4 and K5) in the Kestanbol geothermal field (Figure 1b). A total of 30 water samples were collected in 6 different periods (July, October 2018 and January, February, April, and July 2019) during the years 2018 and 2019. The location and elevation above sea level of the sampling points were recorded with a handheld global positioning system (Garmin GPSMAP 62s, Garmin International, Kansas, USA). The temperature, electrical conductivity (EC), salinity, and pH measurements were carried out in the field using a WTW Multi 340i pH/conductivity measuring instrument (Wissenschaftlich-Technische Werkstätten, Weilheim, Germany). The probes were calibrated in accordance with manufacturer's recommendations on the day of field study. The flow rate of cold springs was measured in the field. Water samples were filtered into polyethylene bottles (100 mL × 2) using syringe-filtered 0.45 µm nitrocellulose filters (Millipore, Merck, Darmstadt, Germany). One bottle was acidified with reagent-grade nitric acid (Merck, Darmstadt, Germany) to pH ≤ 2.0 for determination of cations, and the other was left unacidified for anion analyses. For $\delta^{18}O$, $\delta^{2}H$, and ^{3}H analysis, water samples were collected seasonally (October 2018 and April 2019) and stored in 1000 mL polyethylene bottles. All water samples were stored in a refrigerator at 4 °C until analysis.

2.2. Laboratory studies

Major cations and selected elements (Na^{+}, K^{+}, Ca^{2+}, Mg^{2+}, B, Ba, Fe and Mn) were analyzed using an inductively coupled plasma optical emission spectroscopy (ICP-OES, Optima 8000, PerkinElmer, Waltham, Massachusetts, USA). The major anions (SO_4^{2-} and Cl^{-}) were analyzed by ion chromatography (IC, LC-20A SP, Shimadzu, Kyoto, Japan). The ICP-OES and IC analyses were performed at the Science and Technology Application and Research Center at Çanakkale Onsekiz Mart University (Çanakkale, Turkey). The detection limits for analyzed cations and anions were as follows: Na^{+} (0.1 mg/L), K^{+} (0.1 mg/L), Ca^{2+} (0.1 mg/L), Mg^{2+} (0.1 mg/L), B (50 g/L), Ba (25 g/L), Fe (25 g/L), Mn (50 g/L), SO_4^{2-} (1 mg/L) and Cl^{-} (1 mg/L). The concentrations of bicarbonate in the water samples were measured by titration. The ion balance between anions and cations was calculated in meq/L to less than 5%.

The $\delta^{18}O$ and $\delta^{2}H$ of the water samples were determined using the optic method developed by the International Atomic Energy Agency (IAEA) with wavelength-scanned cavity ring-down spectroscopy (L2130-i, Picarro, Santa Clara, California, USA). The ^{3}H measurements were determined using an ultra low-level liquid scintillation spectrometer (Quantulus 1220, PerkinElmer, Waltham, Massachusetts, USA). Analyses for $\delta^{18}O$, $\delta^{2}H$, and ^{3}H in water samples were carried out at the General Directorate of State Hydraulic Works-Technical Research and Quality Control Department of Isotope Laboratory (Ankara, Turkey). The O and H isotopic ratios are expressed relative

to Vienna Standard Mean Ocean Water (VSMOW). The analytical precision for water analyses was ± 0.15‰ for $\delta^{18}O$, ± 0.82‰ for $\delta^{2}H$, and ± 0.6 TU for ^{3}H values.

3. Results and discussion

3.1. Geological setting

The basement rocks in the Kestanbol geothermal field are represented by the Lower Cambrian Geyikli Formation (Beccaletto, 2003; Beccaletto and Jenny, 2004) (Figure 2a). The Geyikli Formation is composed mainly of metasandstone, phyllite, calcschist and mica schist, and recrystallized limestone. The age of metamorphism in the Geyikli Formation is 531 ± 86 Ma according to Rb/Sr radiometric age of muscovites collected from the mica schists (Duru et al., 2012). The basement rocks are overlain above an unconformity by the Bozalan Formation (Beccaletto and Jenny, 2004; Arik and Aydin, 2011; Duru et al., 2012). The Bozalan Formation consists of dark gray, pink, and white colored bedded recrystallized limestone, phyllite and metasandstone. According to fossil assemblages collected from the upper levels of the Bozalan Formation limestones, the formation age was determined as Middle-Late Permian (Beccaletto and Jenny, 2004; Duru et al., 2012). The Upper Oligocene-Lower Miocene Kestanbol Pluton (Fytikas et al., 1976; Birkle and Satir, 1992; Karacik, 1995; Karacik and Yilmaz, 1995) represented by mainly intensely fractured and cracked quartz-monzonite, monzonite, monzodiorite porphyry, syenite porphyry, and quartz-syenite porphyry was emplaced by cutting all older units (Arik and Aydin, 2011). Akal (2013) stated that the Kestanbol Pluton consists of high-K calc-alkaline to shoshonitic, I-type plutonic rocks and shoshonitic volcanic successions. The pluton is frequently cut by felsic and mafic dykes and contains mafic microgranular enclaves (Sahin et al., 2010). Radiometric studies suggest that age of the Kestanbol Pluton is 28 ± 0.88 Ma identified with the K/Ar method (Fytikas et al., 1984), 21 ± 1.6 Ma with the K/Ar method (Birkle and Satir, 1995), and 22.8 ± 0.2 Ma with the Ar/Ar method (Altunkaynak et al., 2012). Skarn type mineralization developed along the contact between the Kestanbol Pluton and carbonate rocks of the Bozalan Formation depending on the intrusion of the pluton. Plio-Quaternary fluvial deposits were named Bayramiç Formation (Siyako et al., 1989), which overlies the older units above a disconformity and also consists of slightly cemented red-brown color conglomerate, sandstone, and mudstone. The Quaternary alluvium unconformably overlies all the older units and represents the youngest sedimentary sequence, consisting of slightly consolidated and unconsolidated gravel, sand, clay, and mud transported by Ilica stream.

Based on the lithology and hydrochemical data of the well drilled by MTA (K1), the Kestanbol geothermal field is governed by two major aquifer systems (Olmez, 1976). The primary reservoir rocks in the Kestanbol geothermal field are the partly fractured gneiss at a depth of 60–180 m, and the secondary reservoir is effectively fractured syenite at a depth of 240–290 m (Olmez, 1976). Geothermal water reaches the ground surface through artesian flow. The geothermal waters are heated at depth by the Kestanbol Pluton and high geothermal gradient. Marmara et al. (2020) identified the NE-SW trending right-lateral strike-slip Kaplıca fault parallel to Ilıca stream in the Kestanbol geothermal field. The fault begins at the contact between metamorphics and granites in the east, and it probably ends by continuing under the Aegean Sea in the west, reaching about 10 km in length. Geothermal waters are heated during moderate-deep circulation and ascend to the ground surface through Kaplıca fault and fracture zones within the rocks (Figure 2b). The reduced permeability with increasing depth causes the vertical flow of geothermal water along the permeable fault zone. The Kestanbol geothermal springs are aligned along this NE-SW strike-slip Kaplıca fault. Caglar and Demirorer (1999) reported that resistivity maps and two-dimensional geoelectric models showed a good conductive region about 2 km southwest of Kestanbol geothermal springs. They suggested drilling at a new location down to 100–150 m depth, to produce geothermal water with a higher flow rate.

3.2. Active tectonics and seismicity

The Biga Peninsula is dominantly affected by the tectonic relationship between the strike-slip regime of the NAFZ and the extensional regime of the Aegean (McKenzie, 1972; Dewey and Sengor, 1979; Herece, 1990; Taymaz et al., 1991; Ozden et al., 2018). The NAFZ is composed of a series of right-lateral strike-slip segments extending from eastern Anatolia to the northern Aegean Sea (Ketin, 1948; McKenzie, 1972; Seyitoglu et al., 2016). The NAFZ bifurcates into three branches in the Marmara Region (Dewey and Sengor, 1979; Sengor et al., 1985; Barka, 1997; Gurer et al., 2003; Seyitoglu et al., 2016; Bekler and Demirci, 2018). The north branch of the NAFZ begins southeast of Lake Sapanca passes through İzmit Gulf, Marmara Sea, and Saros Gulf (Sengor et al., 1985; Barka and Kadinsky-Cade, 1988; Herece, 1990; Barka, 1992; Kurcer et al., 2008; Seyitoglu et al., 2016). The central branch follows the path southeast of Lake Sapanca and runs south of Geyve, Pamukova, and Lake İznik extending along the south coast of the Marmara Sea (Kocyigit, 1988; Barka, 1997; Kurcer et al., 2008) and the south branch separates from the central branch near Pamukova and extends in SW-NE direction via Yenişehir, Bursa, Ulubat, Gönen, and Yenice to the Edremit Gulf (Herece, 1990; Yaltirak, 2002; Bekler and Demirci, 2018). The recurrence intervals of earthquakes in the Marmara region affected by the north

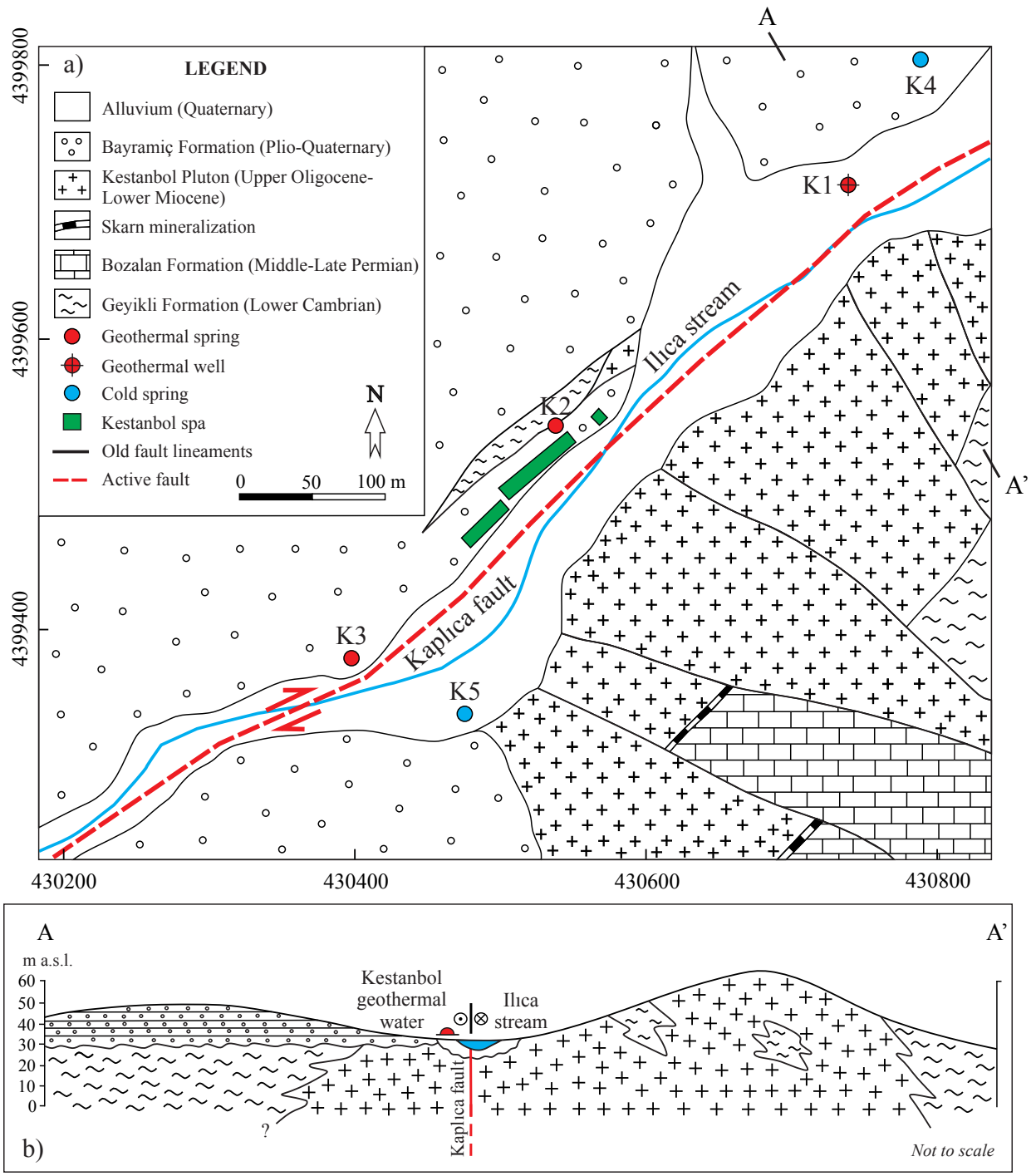

Figure 2. a) Geological map of the Kestanbol geothermal field (modified from Mutzenberg, 1997), b) geological cross-section of the Kestanbol geothermal field.

branch of the NAFZ have short time intervals of 150–300 years, while the central branch is currently a seismic gap and the south branch has a longer earthquake recurrence interval compared to the north branch (Ikeda et al, 1991; Rockwell et al., 2001; Hartleb et al., 2006; Sozbilir et al., 2018). Radiocarbon dates for the earthquakes recorded in trench studies on Yenice-Gönen fault that is considered to be a part of the southern branch of the NAFZ show that the recurrence interval of the earthquakes was calculated as 660 ± 160 years (Kurcer et al., 2008).

The right-lateral strike-slip faults representing the south branch of the NAFZ combined with the West Anatolian extensional regime shaped the active Tuzla, Babakale, Gülpınar, Çamköy and Kestanbol faults (Karacik and Yilmaz, 1998; Emre et al., 2012; Ozden et al., 2018; Sozbilir et al., 2018). These faults play an important role in the distribution of geothermal springs and the development of their hydrogeochemical characterization. The fundamental factor controlling the circulation of geothermal waters in the Kestanbol geothermal field is the Kaplıca fault. In identifying the characteristics of the Kaplıca fault, data for earthquakes larger than Mw ≥ 3.5 occurring in the Kestanbol geothermal field and close surroundings were obtained from Boğaziçi University Kandilli Observatory and Earthquake Research Institute and Boğaziçi University Regional Earthquake-Tsunami Monitoring Center. The focal mechanism solutions for the earthquakes were solved with first arrival polarities and moment tensor inversion methods using zSacWin software. Figure 3 and Table 1 show focal mechanism inversion solutions for some earthquakes around the Kaplıca fault. Based on the determined focal depths, the earthquakes were shallow. From the inverse solutions for the focal mechanisms of these five earthquakes, it is understood that the Kaplıca fault is a right-lateral strike-slip fault with normal component. Additionally, strike is observed to be NE-SW and ENE-WSW. Earthquake data confirm the Kaplıca fault, which was morphologically determined to extend along Ilıca stream in the field.

Several strong and destructive earthquakes occurred on the western part of the NAFZ during historical and instrumental periods. In the historical period (BC 1800-AD 1900), many earthquakes with seismic intensities of up to X occurred along the NAFZ and around Lesvos Island (Soysal et al., 1981). A destructive earthquake occurred on Lesvos Island on March 7, 1867 and the intensity values of the earthquake were reported as X (Papazachos and Papazachou, 2003). The majority of villages in the central part of the island were completely or partly destroyed, and the number of deaths was more than 500 (Roumelioti and Kiratzi, 2010; Papadimitriou et al., 2018). A large earthquake (Mw = 6.7) occurred along the Edremit fault on October 6, 1944 (Ambraseys, 1988). A 38-km long surface rupture developed along the Edremit fault during the earthquake, 73 people died and more than 2200 houses were destroyed (Sozbilir et al., 2016). A strong earthquake (Mw = 7.2) occurred on the Yenice-Gönen fault on March 18, 1953 (Ketin and Roesli, 1953; Pinar, 1953). A surface rupture formed with a length of 70 km between Yenice and Gönen during the earthquake, and 263 people died (Kurcer et al., 2008). The Tuzla fault caused an earthquake swarm in early 2017. Earthquakes continuing over more than three months in Ayvacık, including the January 14, 2017 (Mw = 4.4) and February 6, 2017 (Mw = 5.3) earthquakes, began on the Tuzla fault under the effect of a normal faulting stress regime and migrated southward (Ozden et al., 2018). It was determined that 25 of these earthquakes had Mw = 4 and above. A total of 1470 buildings were extensively damaged in Ayvacık (Livaoglu et al., 2018). Sozbilir et al. (2018) suggested that the Tuzla fault can produce the energy of a 6.7 Mw earthquake. From July 2018 to June 2019, 20 earthquakes with Mw = 3.5 and above occurred in the close surroundings of the Kestanbol geothermal field (Table 2, Figure 4). The most significant of these earthquakes was the February 20, 2019 Tartışık-Ayvacık earthquake (Mw = 5.0). During our monitoring period, no earthquake occurred on the Kaplıca fault.

3.3. Hydrogeochemistry

3.3.1. Physicochemical and chemical characterization

The temperature varied from 59.5 to 74.6 °C in geothermal waters with a mean value of 68.13 °C, and from 11.2 to 25.4 °C in cold waters with a mean value of 17.39 °C (Table 3). The flow rates of the cold waters ranged from 0.2 to 0.7 L/s. The geothermal waters were slightly acidic, with pH values ranging between 6.13 and 6.83. In contrast, the cold waters were alkaline, with pH values from 7.35 to 8.08. The salinity of geothermal and cold waters varied from 19.6 to 23.3‰ and 0 to 0.7‰, respectively. The EC of geothermal and cold waters were between 30300 and 35700 µS/cm and between 710 and 1690 µS/cm, respectively. Cam et al. (2013) reported that pH value, EC, and salinity of the Aegean Sea were 8.25, 58200 µS/cm, and 38.6‰, respectively (Table 4). The total dissolved solids (TDS) in Kestanbol geothermal waters ranged from 20875 to 23535 mg/L (Mutzenberg, 1997), indicating geothermal waters are saline. Kavouridis et al. (1997) reported that TDS value for Aegean Sea was 40979 mg/L.

According to the International Association of Hydrogeologists (IAH, 1979) classification, geothermal and cold waters were Na-Cl and Ca-HCO_3-Cl water types, respectively. The major ion concentrations were plotted on Piper (1944) and Schoeller (1955) diagrams (Figures 5a, 5b). According to the classification in the Piper diagram, the geothermal and cold waters plotted in different fields. The major ion sequence of cold waters generally was $Ca^{2+} > Na^{+} > Mg^{2+} > K^{+}$ and $HCO_3^{-} > Cl^{-} > SO_4^{2-}$. The low mineralized cold waters represent the outflow of local groundwater recharging and circulating in the fissured rocks of the intrusion of the Kestanbol Pluton. The Schoeller diagram suggests that geothermal waters originate in the same geothermal aquifer. The sequences of major cations and anions in geothermal waters generally were as follows: $Na^{+} > Ca^{2+} > K^{+} > Mg^{2+}$ and $Cl^{-} > HCO_3^{-} > SO_4^{2-}$, respectively. The dominant cation in geothermal water was Na^{+} with concentrations ranging from 5358 to 7572 mg/L with a mean of 6500 mg/L, accounting for 80% of total cations. The Cl^{-} was the most abundant

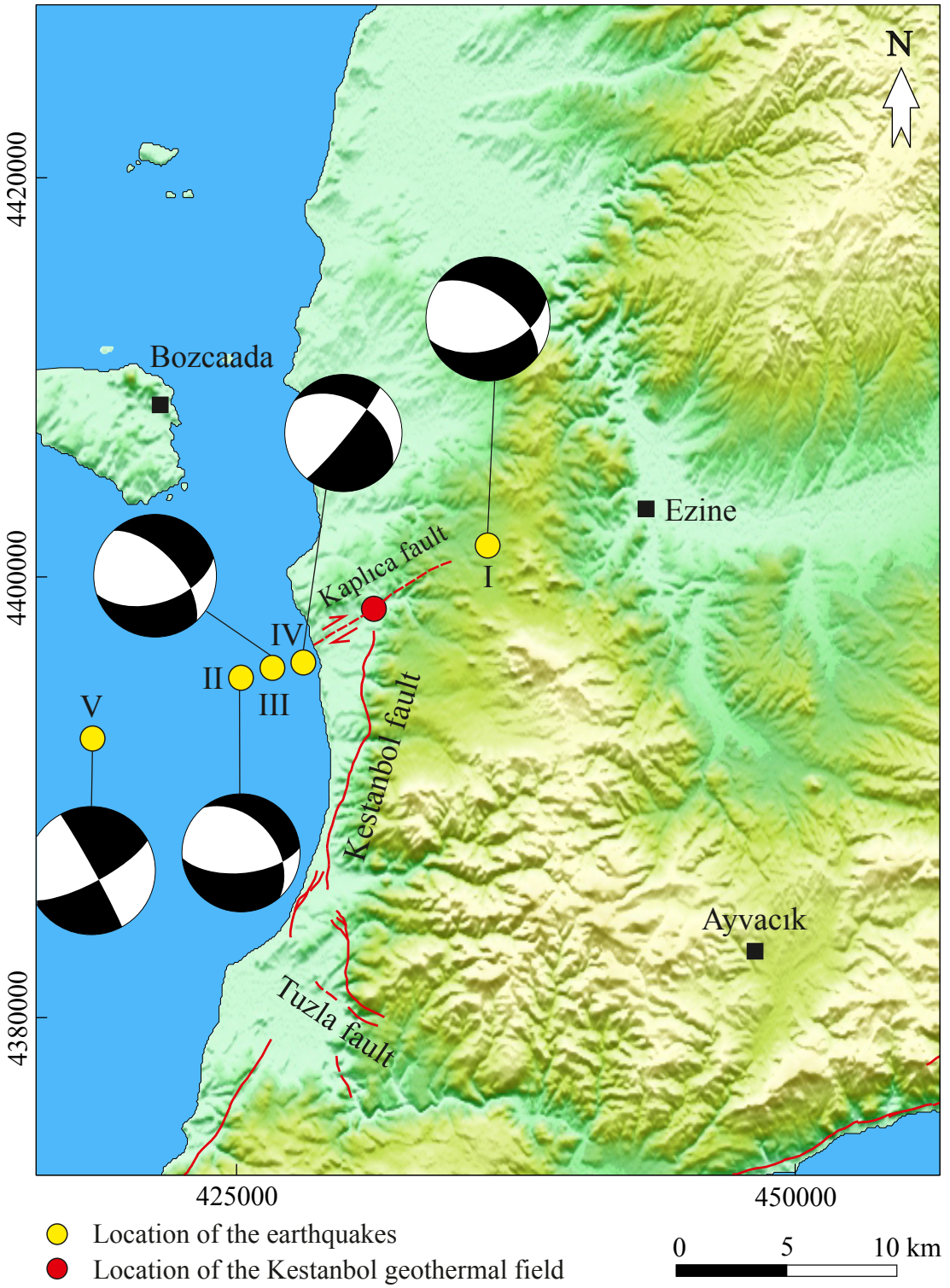

Figure 3. The focal mechanism solutions of some earthquakes that occurred around the Kaplıca fault.

anion in geothermal waters, with concentrations ranging from 10316 to 13507 mg/L and a mean of 11987 mg/L, accounting for 97% of total anions.

Baba and Ertekin (2007) and Cam et al. (2013) stated that the NaCl concentration of the Aegean Sea was 40926 and 33430 mg/L, respectively. Marine sources of

Table 1. The focal mechanism solutions of some earthquakes that occurred in the vicinity of the Kaplıca fault (UTM Zone 35).

No	I	II	III	IV	V
Date	10/26/2015	1/7/2014	1/7/2014	1/6/2014	9/12/2008
Time	23:07:59	21:41:21	01:47:46	10:23:38	02:12:42
Easting (m)	435399	424614	426130	427248	418266
Northing (m)	4402526	4395286	4396044	4396552	4393189
Depth (km)	6.0	7.1	6.2	7.9	9.1
Magnitude (Mw)	4.4	4.1	3.5	3.9	4.1
Strike 1	71	85	39	73	62
Dip 1	49	62	84	53	75
Rake 1	–133	–123	–133	–141	–177
Strike 2	320	305	303	317	331
Dip 2	42	56	43	60	87
Rake 2	–44	–52	–9	–44	–15

Table 2. The parameters of the 20 earthquakes (Mw ≥ 3.5) affecting Kestanbol geothermal field between July 2018 and June 2019 (UTM Zone 35).

Name	Date	Time	Easting (m)	Northing (m)	Depth (km)	Magnitute (Mw)	Location
A	7/18/2018	22:56:07	416659	4378262	7.5	3.5	Gülpınar
B	10/23/2018	17:57:02	418050	4347169	7.0	3.8	Lesvos Island
C	12/17/2018	17:40:55	427808	4375930	7.4	3.9	Yukarıköy-Ayvacık
D	12/28/2018	19:12:45	428657	4374812	6.1	3.7	Yukarıköy-Ayvacık
E	01/14/2019	09:59:35	373300	4354428	8.7	3.9	Aegean Sea
F	01/28/2019	19:58:34	430296	4365918	5.4	3.5	Koyunevi-Ayvacık
G1	02/20/2019	21:23:27	451076	4385737	7.6	5.0	Tartışık-Ayvacık
G2	02/20/2019	22:42:06	450217	4385743	6.3	3.6	Tartışık -Ayvacık
H	03/02/2019	12:51:25	450329	4385305	8.5	3.8	Tartışık -Ayvacık
I	03/13/2019	10:05:24	451927	4384622	7.1	3.5	Tartışık -Ayvacık
J1	03/16/2019	00:54:18	377471	4399878	5.4	4.5	Aegean Sea
J2	03/16/2019	03:58.23	382595	4398687	9.2	3.6	Aegean Sea
K1	03/20/2019	03:20:16	375721	4397685	4.6	3.5	Aegean Sea
K2	03/20/2019	09:59:35	376596	4398781	5.1	3.5	Aegean Sea
L1	04/29/2019	21:02:43	441441	4360277	12.0	4.3	Edremit Gulf
L2	04/29/2019	21:39:50	441304	4359783	10.7	3.6	Edremit Gulf
M	05/19/2019	21:28:08	374252	4359963	9.0	3.7	Aegean Sea
N1	06/06/2019	06:24:11	371430	4345577	9.5	3.6	Aegean Sea
N2	06/06/2019	20:14:17	376579	4397671	5.0	3.7	Aegean Sea
O	06/17/2019	07:47:30	454542	4391265	13.1	3.9	Misvak-Ayvacık

geothermal water have high NaCl composition, and the Na/Cl ratio is lower than 1 (Vengosh et al., 2002). The mean NaCl concentration of Kestanbol geothermal waters was found to be 18487 mg/L and the ratio of Na/Cl was 0.54. The Na/Cl ratio of geothermal waters were very close to that of seawater. The Kestanbol geothermal waters are enriched in Ca^{2+} and HCO_3^- and depleted in Mg^{2+} and SO_4^{2-} relative to seawater. Vengosh et al. (2002) stated that

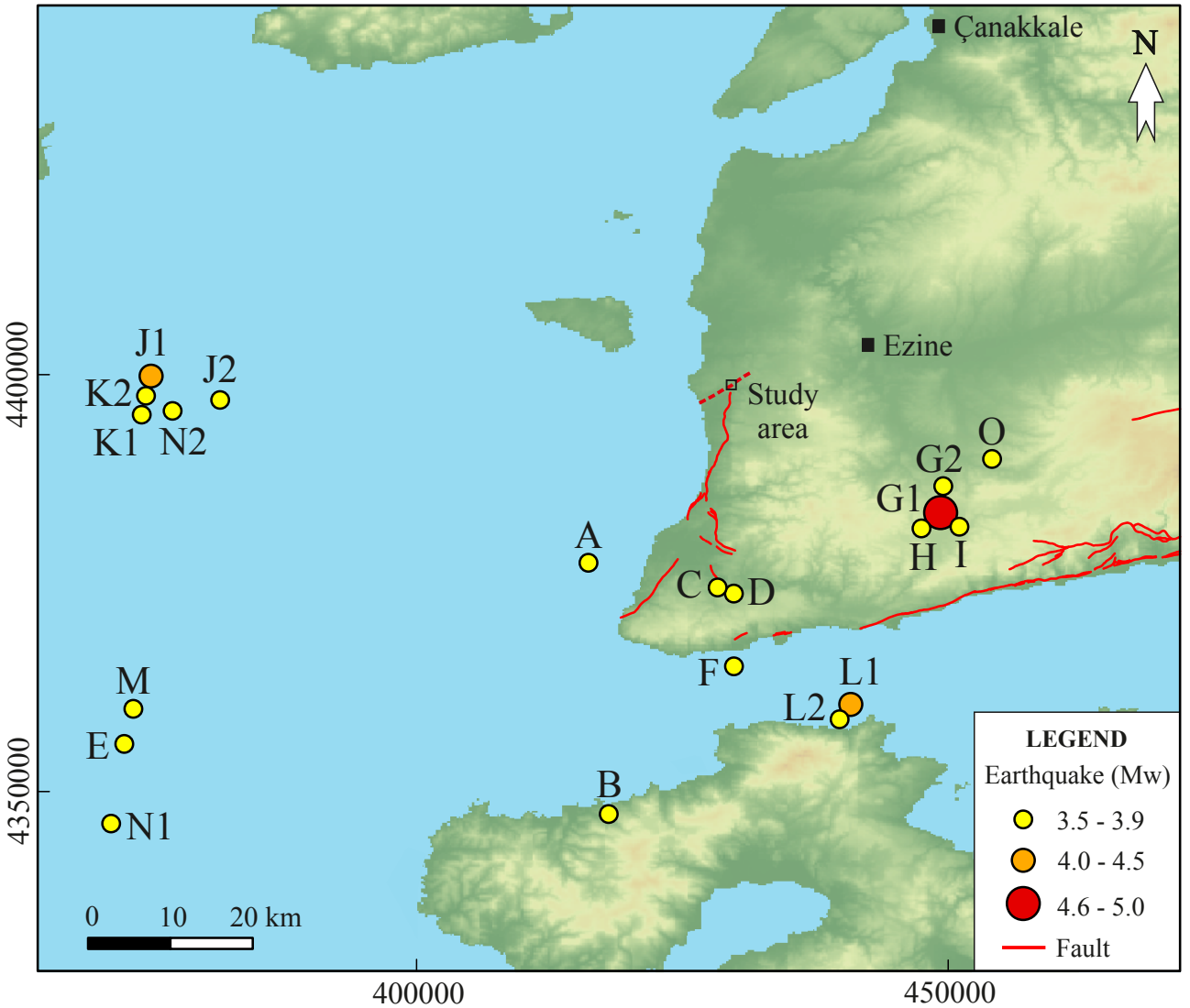

Figure 4. Location map of seismic activities (Mw ≥ 3.5) affecting Kestanbol geothermal field between July 2018 and June 2019.

Cl^- and Br are conservative elements that are less affected by water-rock interactions. The Cl^- and Br have long been used as tracers to determine the origin and evolution of natural waters (Freeman, 2007). Mutzenberg (1997) reported that the Br and Cl^- concentrations in Kestanbol geothermal water were 23 and 13269 mg/L, respectively. The Br/Cl ratio of Kestanbol geothermal waters (1.73×10^{-3}) was lower than the Br/Cl ratio of seawater (3.52×10^{-3}) reported by Goldberg et al. (1971). All Cl^- enriched marine sources of geothermal water have typical Br/Cl ratio lower than seawater (Vengosh et al., 2002). The B/Cl ratio of geothermal waters was calculated as 12.15×10^{-4}. Karaca et al. (2013) reported that Li concentration in Kestanbol geothermal water was 12467 µg/L, and Li/Cl ratio of geothermal water was 9.33×10^{-4}. Cam et al. (2013) reported that B/Cl and Li/Cl ratios for the Aegean Sea were 2×10^{-4} and 3.11×10^{-5}, respectively. The B/Cl and Li/Cl ratios of geothermal waters are higher than those of seawater. The Li is present in significant amounts in igneous rocks, and its average abundance in granite is close to 30 ppm (Krauskopf and Bird, 1995). Due to water-rock interaction, a significant amount of Li was added to geothermal waters. Tokcaer (2007) reported that the $\delta^{11}B$ value of Kestanbol geothermal water was 10.68‰, which is higher than the value expected for B leached from local igneous rocks with $\delta^{11}B \sim 0$‰. The high $\delta^{11}B$ may be explained as seawater ($\delta^{11}B \sim 40$‰) mixing with lower $\delta^{11}B$ values due to water-rock interaction. Mutzenberg (1997) stated that similar Na/Cl ratios and slight differences in B/Cl and Br/Cl ratios between seawater and the Kestanbol geothermal waters suggest altered, fossil seawater as the source of the saline endmember.

Table 3. Chemical composition of geothermal and cold waters in Kestanbol geothermal field.

Sample ID	Sampling date	T	pH	Salinity	EC	Na^+	K^+	Ca^{2+}	Mg^{2+}	Cl^-	HCO_3^-	SO_4^{2-}	B	Ba	Fe	Mn
		°C		‰	µS/cm	mg/L	mg/L	mg/L	mg/L	mg/L	mg/L	mg/L	µg/L	µg/L	µg/L	µg/L
K1	7/14/2018	72.3	6.71	20.1	30900	5921	670	785	64	11389	133	90	10662	1248	6850	1105
	10/25/2018	74	6.5	19.9	30300	7457	862	812	72	12706	300	98	11645	1354	9040	1792
	1/10/2019	74.1	6.61	20.4	31900	7123	709	879	73	12387	240	140	15178	1230	5080	1075
	2/22/2019	73.4	6.66	19.9	31000	6534	596	750	72	11209	260	168	17940	1589	6055	1453
	4/14/2019	73.4	6.7	19.6	30300	5484	478	653	48	10316	266	80	15102	996	4781	1100
	7/17/2019	74.6	6.75	19.7	30400	5358	720	795	53	10635	133	90	15298	1307	2960	1540
K2	7/14/2018	63.1	6.6	21.5	32800	6130	720	845	69	11921	166	90	10436	1418	3060	1348
	10/25/2018	59.5	6.61	21.3	32900	7340	802	819	80	12415	266	122	19115	1508	5139	1650
	1/10/2019	60.6	6.53	20.6	32000	6544	684	956	79	12018	266	120	16832	1410	2941	1256
	2/22/2019	62.5	6.62	20.2	31300	6423	561	770	61	11238	233	170	18740	1753	2016	1517
	4/14/2019	62.4	6.64	20.6	32000	5713	472	637	37	11309	200	80	14959	1171	2337	1600
	7/17/2019	61	6.68	21.3	32500	5944	839	772	58	11894	266	100	14318	1417	2800	1320
K3	7/14/2018	69.5	6.45	23.2	35200	6893	810	961	67	13339	133	100	11765	1556	8800	1450
	10/25/2018	69.4	6.5	23.1	35200	7552	936	795	87	13427	166	108	9310	1754	10962	1837
	1/10/2019	68.9	6.47	23.3	35500	7566	915	1034	71	13472	200	120	16971	1562	10037	1318
	2/22/2019	68.4	6.13	23.3	35500	7572	780	873	73	13507	200	180	16640	2068	11820	1947
	4/14/2019	69	6.19	23.1	35300	5789	550	735	65	11082	300	110	13340	1083	7363	881
	7/17/2019	70.3	6.83	23.2	35700	5663	1058	836	38	11503	333	90	13854	1532	4153	1280
K4	7/14/2018	22.3	7.86	0.3	1090	59	2.59	121	31	153	250	95	52.2	87.51	189.61	55.37
	10/25/2018	15.3	8.08	0.4	1180	65	3.5	118	36	168	270	91	44.8	69.1	330.5	88.12
	1/10/2019	12.1	7.98	0.1	850	70	2.86	129	34	169	293	89	57.5	85.9	332	69.78
	2/22/2019	11.2	7.76	0	930	69	2.7	111	39	174	280	89	61.5	44.5	220.04	56.7
	4/14/2019	14.8	7.54	0	710	77	6	125	19	157	305	97	81.9	35.85	131.3	48.55
	7/17/2019	25.1	7.44	0.3	1040	74	5	145	18	166	296	96	52	51.24	325.3	100.4
K5	7/14/2018	24.2	7.35	0.7	1690	92	4.47	135	28	195	292	87	63.05	107.7	338.1	169.95
	10/25/2018	16.4	7.43	0.7	1680	91	4.76	148	29	184	366	75	50.94	87.1	225.3	165.7
	1/10/2019	12.8	8.06	0.6	1570	85	4.23	144	27	191	325	73	55.7	88.9	286.1	136.9
	2/22/2019	13.3	7.58	0.6	1610	85	4.6	168	22	189	358	81	57.1	92.3	304.7	142.5
	4/14/2019	15.8	7.52	0.2	980	66	4	159	31	169	380	83	72	63.12	262.2	160.8
	7/17/2019	25.4	7.39	0.7	1540	65	6.2	166	46	204	390	85	65.8	105.88	291.2	165.5

Table 4. Chemical composition of Kestanbol geothermal waters and seawater in the literature.

Sample ID	References	T	pH	Salinity	EC	Na^+	K^+	Ca^{2+}	Mg^{2+}	Cl^-	HCO_3^-	SO_4^{2-}	B	Ba	Fe	Mn
		°C		‰	µS/cm	mg/L	mg/L	mg/L	mg/L	mg/L	mg/L	mg/L	µg/L	µg/L	µg/L	µg/L
K1	Mutzenberg (1997)	76.2	5.9	na	23900	6570	804	828.7	61.8	12319	292.2	96	na	1600	1100	1400
		76.1	na	na	24700	6220	904	835.7	45	12230	291	77	na	1300	6200	1300
		na	6.5	na	na	6920	799	807.2	59.3	12832	286.1	103	na	na	na	na
K2		63.6	6.2	na	25500	6310	866	882.8	62.6	13294	302.6	92	na	1700	1200	1500
		64.1	na	na	27000	6910	949	927.9	49.8	13382	309.3	67	na	1400	2800	1500
K3		70.5	5.9	na	27400	6700	903	938.7	68	13269	305.6	91	na	1900	1200	1900
		69.8	na	na	27700	7200	981	959.9	52.3	13684	310.5	80	na	1500	9200	1600
K1	Baba and Ertekin (2007)	68	6.2	na	na	7316	825	1143.8	78.7	13321	320	150	12720	na	na	na
		66	6.4	na	na	6343	735.2	858.5	62.42	13207	291	143	10700	na	na	na
K1	Tokcaer (2007)	75.6	7.08	na	33000	6150	645	860	56	12800	366.1	177.5	12260	na	5200	1400
K1	Karaca et al. (2013)	75.3	6.2	20.7	31700	6788	812	976.2	74	13285	156.67	150	13964	1579	na	1441
K2		69.2	5.8	23.4	35200	7276	917	1060	78	13157	163.33	150	14884	1807	14998	1695
K3		70.4	5.9	21	32200	7452	912	1063	79	13353	166.67	140	15017	1733	11417	1678
Seawater	Goldberg et al. (1971)	na	na	na	na	10500	390	410	1350	19000	142	2700	4500	20	3	2
Aegean Sea	Baba and Ertekin (2007)	17.8	8.3	na	na	14600	565.7	629.3	1897.7	26326	488	na	na	na	na	na
	Cam et al. (2013)	18.1	8.25	38.6	58200	10934	690	438	1415	22496	146	3246	4500	na	na	na

Note: na indicates not analyzed.

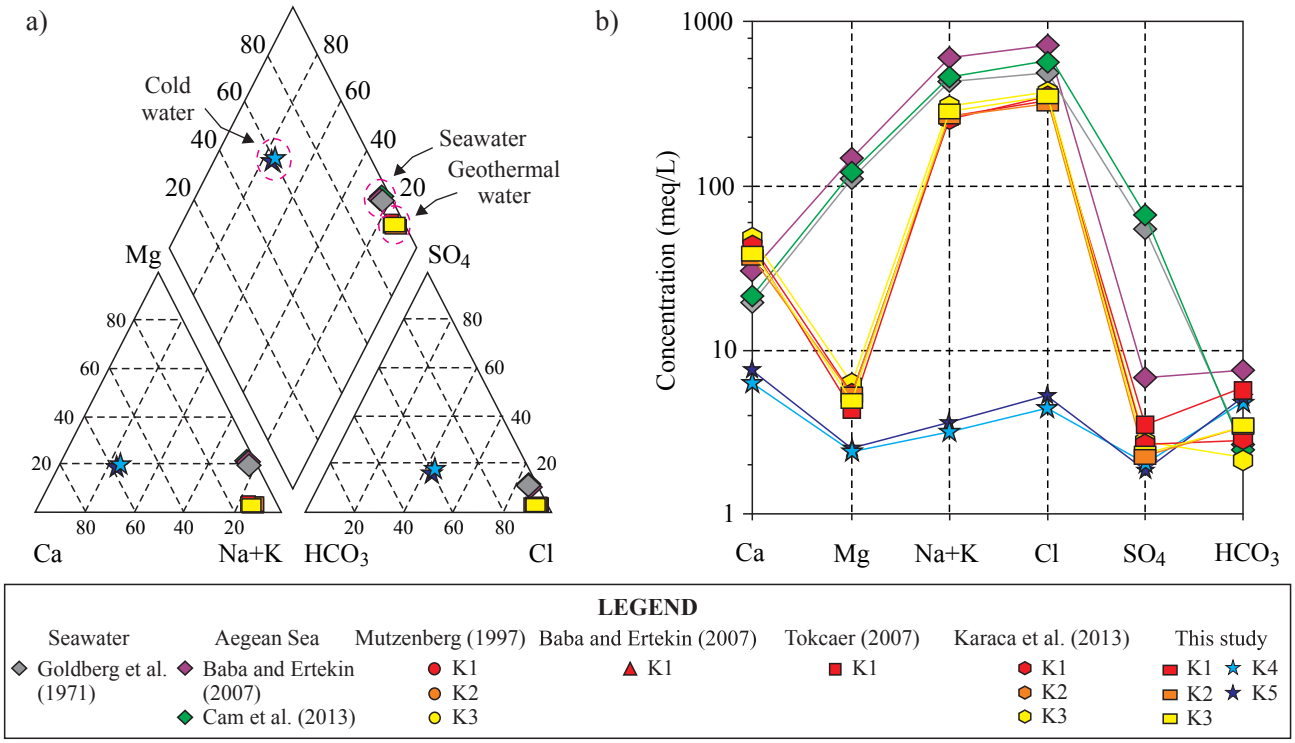

Figure 5. Distribution of geothermal and cold waters and seawater in a) Piper ternary diagram, b) Schoeller semilogarithmic diagram.

The surroundings of the Kestanbol geothermal springs are well characterized by calcite, halite, and siderite scaling (Marmara et al., 2020). Scales are generally observed with yellow and orange, and occasionally white color in the field. Marmara et al. (2020) reported that the As, Fe and Mn concentrations of scale are higher than the mean values for the continental crust defined by Krauskopf and Bird (1995). Kestanbol geothermal waters are highly mineralized with elevated levels of As, Ba, Fe, and Mn. The maximum Ba, Fe, and Mn concentrations in Kestanbol geothermal waters were measured as 2068, 11820, and 1947 µg/L, respectively. Baba and Ertekin (2007) stated that the As concentration in Kestanbol geothermal waters was 101 µg/L. Goldberg et al. (1971) reported that the As, Ba, Fe, and Mn concentrations in seawater were 3, 20, 3, and 2 µg/L, respectively. The As, Ba, Fe and Mn concentrations in geothermal waters are much higher than those of seawater, indicating that seawater is not the primary source for these elements. The long-term deep circulation of geothermal waters along the Kaplıca fault allows more extensive water-rock interactions. The high concentrations of elements in geothermal waters are derived from water-rock interaction processes under high-temperature conditions. Since Kestanbol geothermal waters are not filtered or reinjected after being used in the spa, the discharge of geothermal waste water has resulted in thermal and chemical contamination of soil and waterways (Marmara et al., 2020). The maximum concentration of B, Ba, Fe and Mn in cold waters were determined as 81.9, 107.7, 338.1, and 169.95 µg/L, respectively. The concentration of Fe and Mn in cold waters exceeded the maximum permissible limits of 200 and 50 µg/L, respectively, recommended by the water intended for human consumption standard (TS266, 2005) in Turkey.

3.3.2. Chemical geothermometer applications

Various chemical geothermometers are used to estimate reservoir temperatures of geothermal systems and determine effective use of geothermal waters (Fournier, 1977; Sanliyuksel and Baba, 2011; Temizel and Gultekin, 2018). These geothermometers assume that the equilibrium of chemical compositions attained in the geothermal reservoir is maintained during the ascent of geothermal waters from a deep reservoir to the surface (Karingithi, 2009; Mao et al., 2015; Hsu and Yeh, 2020).

The ternary diagram of $Na/1000\text{-}K/100\text{-}Mg^{1/2}$ developed by Giggenbach (1988) is used to estimate the reservoir temperatures and identify the maturity of rocks in contact with water. All of the geothermal waters in this study fall in the area of partly equilibrated or mixed waters when plotted on the diagram of Giggenbach (Figure 6). The diagram demonstrates that none of the geothermal waters reached full equilibrium with the host rocks. The Na-K geothermometers (Fournier and Truesdell, 1973; Fournier, 1979; Arnórsson et al., 1983) gave unreasonable

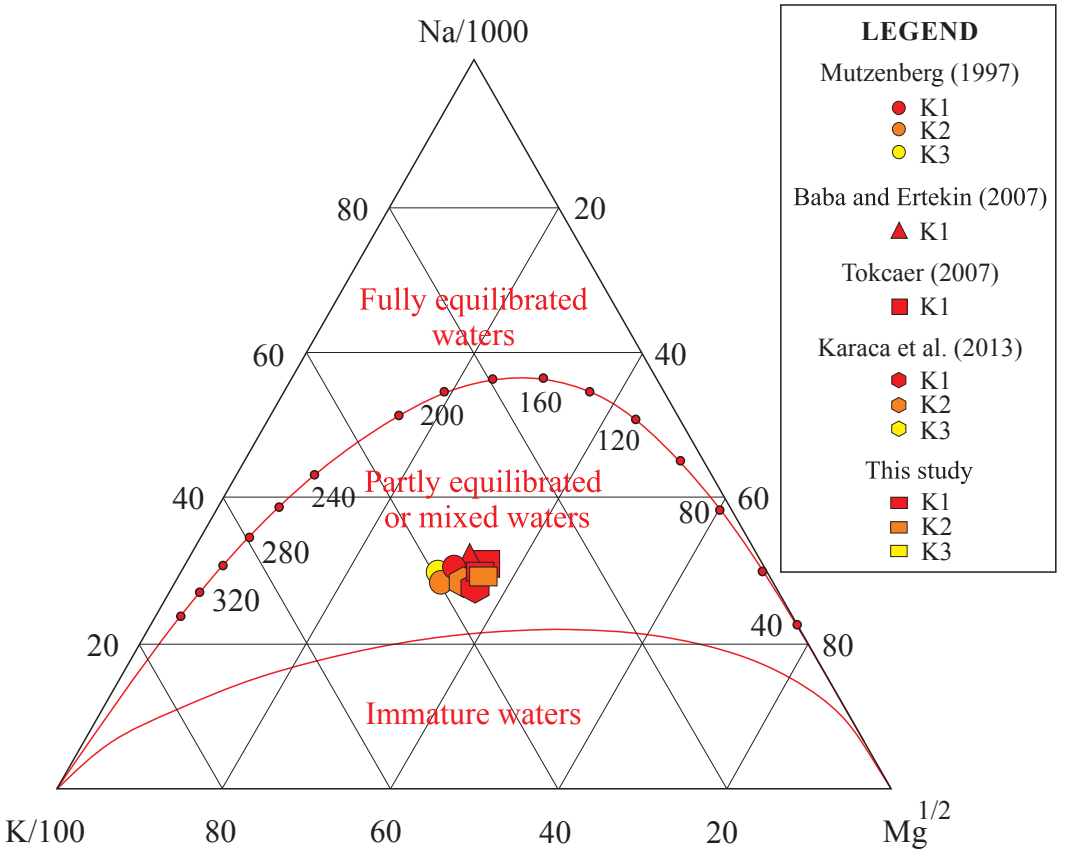

Figure 6. The Na-K-Mg ternary diagram (Giggenbach, 1988) showing estimated reservoir temperatures.

reservoir temperatures of more than 200 °C, probably due to altered seawater intrusion into the reservoir. The reservoir temperature of geothermal waters was calculated using the Na-Li geothermometer proposed by Fouillac and Michard (1981) as 126–139 °C. The K-Mg geothermometer proposed by Giggenbach (1988) was also applied and reservoir temperature was calculated in the range of 161–180 °C.

Mutzenberg (1997), Baba and Ertekin (2007) and Tokcaer (2007) determined that the SiO_2 concentrations of Kestanbol geothermal waters were between 105.03 and 143.75 mg/L (Table 5). Quartz geothermometers are generally used for geothermal waters with temperatures ranging from 150–225 °C, whereas chalcedony geothermometers are used for temperatures lower than 180 °C (Fournier, 1977; Davalos-Elizondo et al., 2021). Hence, the temperatures (111 to 134 °C) obtained from chalcedony geothermometers were more reasonable than those from quartz geothermometers (138 to 158 °C). The β-cristobalite and amorphous silica geothermometer results were ignored because of calculating lower values than the discharge temperatures. At temperatures less than 180 °C, the solubility of silica is usually controlled by chalcedony rather than quartz (Belhai et al., 2016). Consequently, the chalcedony geothermometer with a mean value of 121 °C was the most appropriate silica geothermometer to estimate reservoir temperature of the Kestanbol geothermal waters.

3.3.3. Environmental isotopes

The $\delta^{18}O$, $\delta^{2}H$ and ^{3}H analyses of geothermal and cold waters were performed in rainy and dry seasons (Table 6). In addition, some isotopic data for Kestanbol geothermal waters collected from previous studies (Mutzenberg, 1997; Baba and Ertekin, 2007; Tokcaer, 2007; Karaca et al., 2013) were included for further analysis. The geothermal waters have $\delta^{18}O$ and $\delta^{2}H$ values that range from –5.65 to –4.77‰ and from –38.48 to –33.38‰ (N = 18), respectively. The cold waters have $\delta^{18}O$ values ranging from –6.89 to –6.4‰ and $\delta^{2}H$ values ranging from –41.45 to –37.18‰. Sanliyuksel Yucel et al. (2016) determined the $\delta^{18}O$ and $\delta^{2}H$ values of local rainwater falling in the southeast of Çanakkale were –5.91‰ and –38.29‰, respectively. Cam et al. (2013) reported that $\delta^{18}O$ and $\delta^{2}H$ values for the Aegean Sea were 1.33 and 10.13‰, respectively.

The correlation between $\delta^{18}O$ and $\delta^{2}H$ values in the geothermal and cold waters was plotted on Figure 7, in

Table 5. Estimated reservoir temperatures of Kestanbol geothermal waters using silica geothermometers °C.

Sample ID	References	SiO_2 (mg/L)	Q^a	Q^b	Q^c	C^b	C^d
K1	Mutzenberg (1997)	139.3	156	156	156	132	128
		115.7	145	145	144	119	117
K2		124.3	149	149	148	124	121
		109.3	142	142	140	116	114
K3		132.9	153	153	153	128	125
		109.3	141	141	140	115	113
K1	Baba and Ertekin (2007)	143.75	158	158	158	134	130
		115.52	145	145	144	119	117
K1	Tokcaer (2007)	105.03	140	139	138	113	111

Note: Q: quartz, C: chalcedony, a: Fournier and Potter (1982), b: Fournier (1977), c: Verma (2000), d: Arnórsson et al. (1983).

Table 6. Isotopic composition of geothermal and cold waters.

Sample ID	References	$\delta^{18}O$ (‰)	$\delta^{2}H$ (‰)	^{3}H (TU)
K1	Mutzenberg (1997)	–5.18	–37.5	< 0.9
		–5.09	–37	na
K2		–4.98	–36.5	< 0.7
		–4.88	–35.4	na
K3		–5.09	–37.5	< 1.2
		–5.11	–37.6	na
Tuzla geothermal well		–1.7	–22.6	< 1.3
K1	Baba and Ertekin (2007)	–5.65	–33.38	0.22
		–5.12	–33.62	0.25
K1	Tokcaer (2007)	–4.77	–35.4	na
K1	Karaca et al. (2013)	–5.06	–36.74	na
K2		–5.09	–38.48	na
K3		–5.01	–36.37	na
K1	This study (10/25/2018)	–5.51	–36.89	0.08
K2		–5.15	–35.67	0
K3		–5.21	–35.95	0.18
K4		–6.4	–37.18	0.51
K5		–6.44	–37.56	0.5
K1	This study (4/14/2019)	–5.41	–36.28	0
K2		–5.23	–35.4	0.3
K3		–5.19	–35.9	0.46
K4		–6.89	–41.45	4.91
K5		–6.83	–40.68	3.35
Aegean Sea	Cam et al. (2013)	1.33	10.13	1.1
Nisyros island, NIS2 geothermal well	Dotsika (1991)	4.1	–2.1	na
		1.7	–0.9	na
	Kavouridis et al. (1999)	3.3	–4.25	na

Note: na indicates not analyzed.

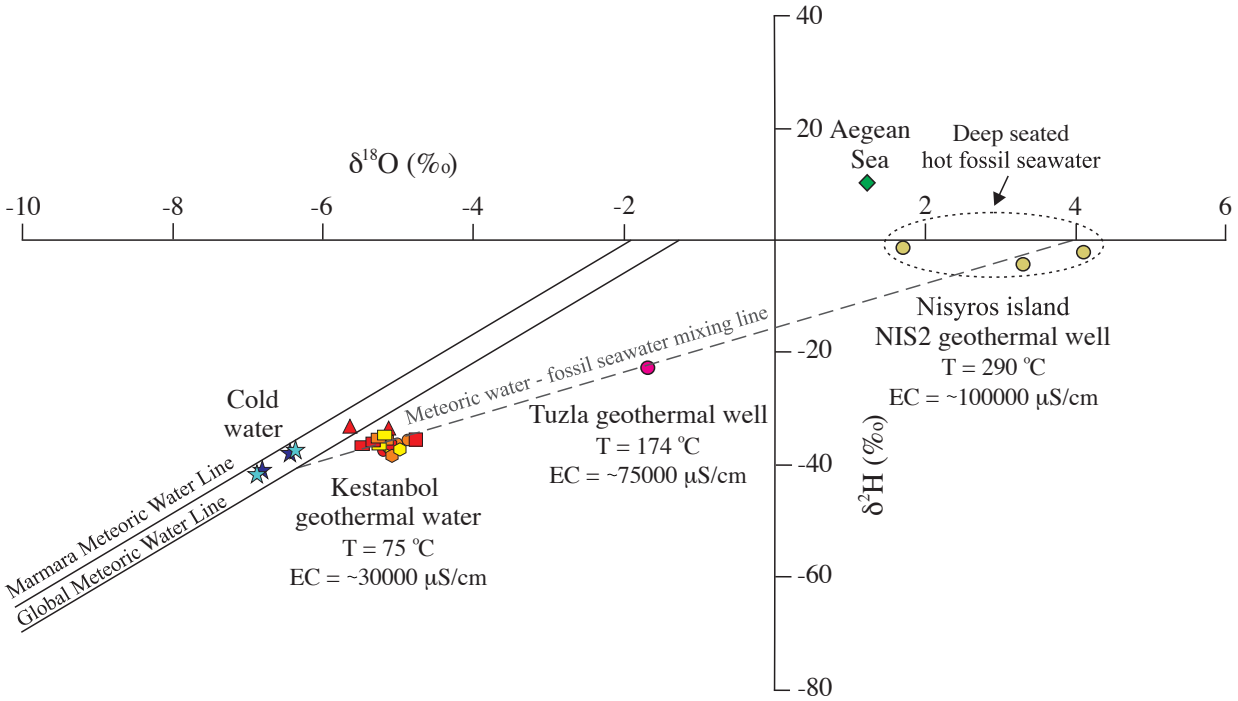

Figure 7. The plot of $\delta^{18}O$ vs. $\delta^{2}H$ (VSMOW) (modified from Yalcin, 2007).

comparison with the Global Meteoric Water Line (GMWL, $\delta^{2}H‰ = 8 \times \delta^{18}O‰ + 10$; Craig, 1961) and the Marmara Meteoric Water Line (MMWL, $\delta^{2}H‰ = 8 \times \delta^{18}O‰ + 15$; Eisenlohr, 1997). Mutzenberg (1997) stated that Tuzla (20 km south of Kestanbol) and Kestanbol geothermal waters probably have the same origin, since a similar chemical composition is observed in both geothermal systems. The isotopic values published from deep wells in Tuzla and Nisyros Island (15 km from the Turkish coast, Greece) were plotted into the $\delta^{2}H$-$\delta^{18}O$ diagram. Mutzenberg (1997) reported that $\delta^{2}H$ and $\delta^{18}O$ values of the Tuzla geothermal well was –1.7 and –22.6‰ at 174 °C, respectively. The samples collected from the NIS2 deep well yielded isotopic compositions of –2.1 and 4.1%, for $\delta^{2}H$ and $\delta^{18}O$, respectively, for the liquid phase, and –0.9 and 1.7% for $\delta^{2}H$ and $\delta^{18}O$, respectively, for the separated steam (Dotsika, 1991). Deep brine at 330 °C was calculated to be –4.25 and 3.3%, for $\delta^{2}H$ and $\delta^{18}O$, respectively by Kavouridis et al. (1999). The low mineralized cold waters plotted between GMWL and MMWL, indicating meteoric origin. The cold waters have the same recharge area, shallow circulation, and are also affected by seasonal variations depicted by their $\delta^{18}O$ and $\delta^{2}H$ data. The $\delta^{18}O$ and $\delta^{2}H$ values of geothermal waters are more positive with respect to the cold waters. The geothermal waters are slightly shifted to the right of the GMWL and fall to the line that represents mixing and dilution between brines of the Nisyros and local groundwater. The plotted $\delta^{18}O$ and $\delta^{2}H$ values of meteoric waters, Kestanbol and Tuzla geothermal waters are positively correlated with the NIS2 geothermal well ($R^{2} = 0.95$). Yalcin (2007) explained the origin of Kestanbol geothermal water is a deep-seated hot fossil seawater that is diluted and cooled during movement and flushing of infiltrating meteoric water.

The ^{3}H is a radioactive isotope of hydrogen with a relatively short half-life of 4500 ± 8 days (Lucas and Unterweger, 2000), and ^{3}H is used as a natural tracer to estimate the residence time of water in the ground (Michel, 2005; Kralik, 2015). The ^{3}H concentration measurements at nine monitoring stations (Adana, Ankara, Antalya, Diyarbakır, Edirne, Erzurum, İzmir, Sinop and Rize) were carried out for 345 precipitation samples during 2012–2016 in Turkey (Dilaver et al., 2018). The results showed that the concentrations of ^{3}H varied from 1.42 to 15.54 TU with a mean of 6.22 TU. The ^{3}H content of precipitation increases in the winter months to the beginning of summer, with the maximum ^{3}H values measured during May and June in Turkey. This increase is controlled by the transition of ^{3}H from the stratosphere-troposphere boundary to the troposphere where weather events occur (Dilaver et al., 2018).

The ^{3}H contents of cold waters varied from 0.5 to 0.51 TU in October 2018 and 3.35 to 4.91 TU in April 2019. The observed variability for the cold waters from 0.5 to 4.91 TU for ^{3}H reflects seasonal variations affecting the meteoric waters. Baba and Ertekin (2007) reported that ^{3}H content of K1 was measured as 0.22 and 0.25 TU. The ^{3}H content of geothermal waters varied from 0 to 0.18 TU in October 2018 and 0 to 0.46 TU in April 2019. The amount of ^{3}H

in water can be used to qualitatively determine whether the groundwater is modern or not (Barbier et al., 1983; Clark and Fritz, 1997; Temizel and Gultekin, 2018). The ^{3}H values equal to or greater than 1 TU are accepted as modern water; moreover, ^{3}H concentrations below 1 TU show that groundwater was recharged prior to the period of atmospheric testing of thermonuclear weapons (Ravikumar and Somashekar, 2011). The ^{3}H values of geothermal waters were below 0.46 TU indicating the system was recharged before the 1950s. The low ^{3}H contents of the geothermal waters suggest that these geothermal waters have deeper circulation and longer residence times than the cold waters.

3.4. The effect of active tectonics on the hydrogeochemistry

In the literature, many different researchers stated that there are temporary or permanent hydrogeochemical changes in geothermal waters prior to and/or after earthquakes with Mw ≥ 5 (Song et al., 2005; Italiano et al., 2010; Du et al., 2010; Chen et al., 2014). Within the scope of this study, the K1 geothermal well drilled by MTA and independent of atmospheric conditions was chosen to determine the effect of the active tectonic regime on hydrogeochemical changes in Kestanbol geothermal water. In 6 different sampling periods from July 14, 2018 to July 17, 2019, the hydrogeochemical characterization of geothermal water was investigated before and after earthquakes. Additionally, 2 days after the Tartışık-Ayvacık earthquake (Mw = 5.0), physicochemical parameter measurements and water sampling were performed from K1.

Variations were observed in the temperature, EC and pH values of geothermal water before and after earthquakes (Figure 8). After the Tartışık-Ayvacık earthquake, the temperature of the geothermal water reduced by 0.7 °C and EC reduced by 900 µS/cm, while the pH value increased by 0.05. After the Tartışık-Ayvacık earthquake, the concentrations of Na^{+}, K^{+}, Ca^{2+}, Mg^{2+} and Cl^{-} reduced, and concentrations of SO_4^{2-}, HCO_3^{-}, B, Ba, Fe and Mn were identified to increase in geothermal water (Figure 9). The most probable reasons for these variations are the nature and dynamics of the thermal circulation system, atmospheric conditions, weathering processes, and groundwater regimes (Yalcin et al., 2003). Shallow circulation and deep circulation create different favorable conditions for element migrations (Belin et al., 2002). As Cl^{-} is considered to be a conservative constituent of the geothermal waters, the decrease in the Cl^{-} concentration points to a geothermal-cold water mixing process and seems to be related to the increased seismic activity. The decrease in the temperature and EC of geothermal water after the Tartışık-Ayvacık earthquake also supports these data. The levels of variations from the original concentrations became less noticeable with time.

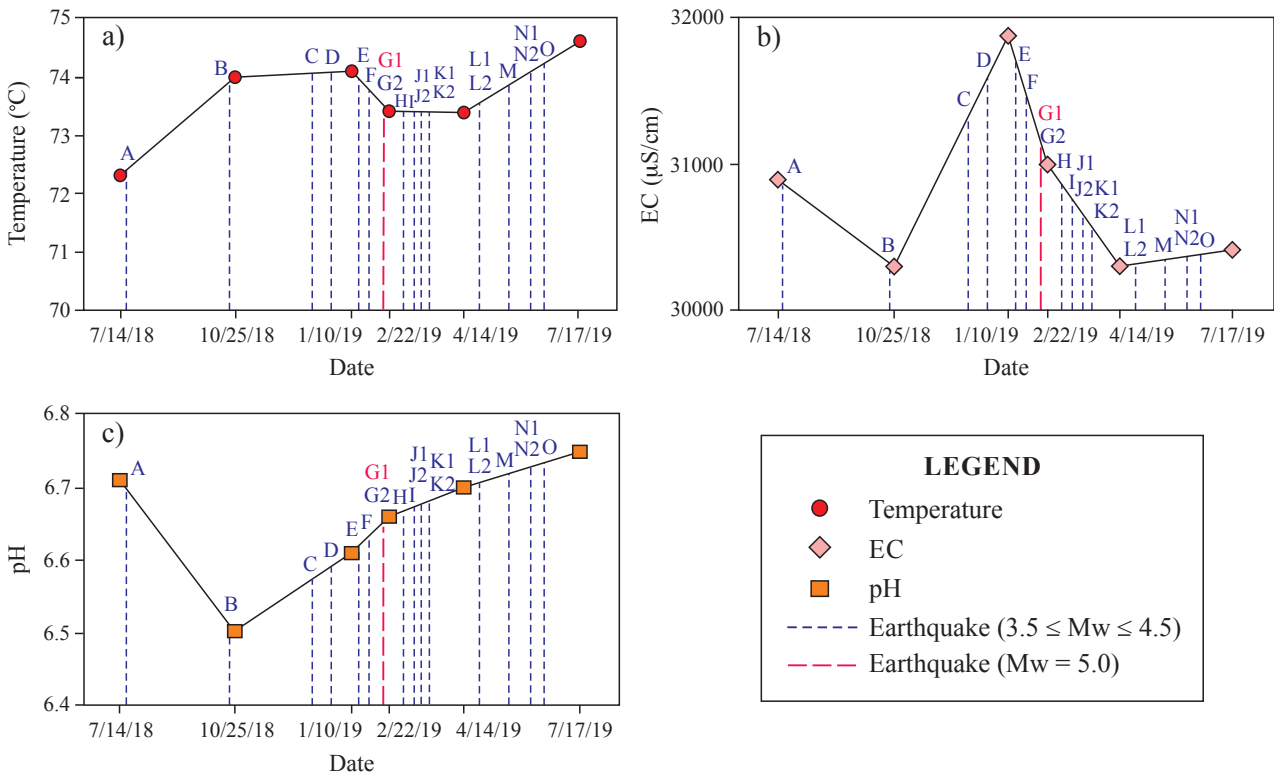

Figure 8. Temporal variations of a) temperature, b) EC, and c) pH value in Kestanbol geothermal water connected with seismicity.

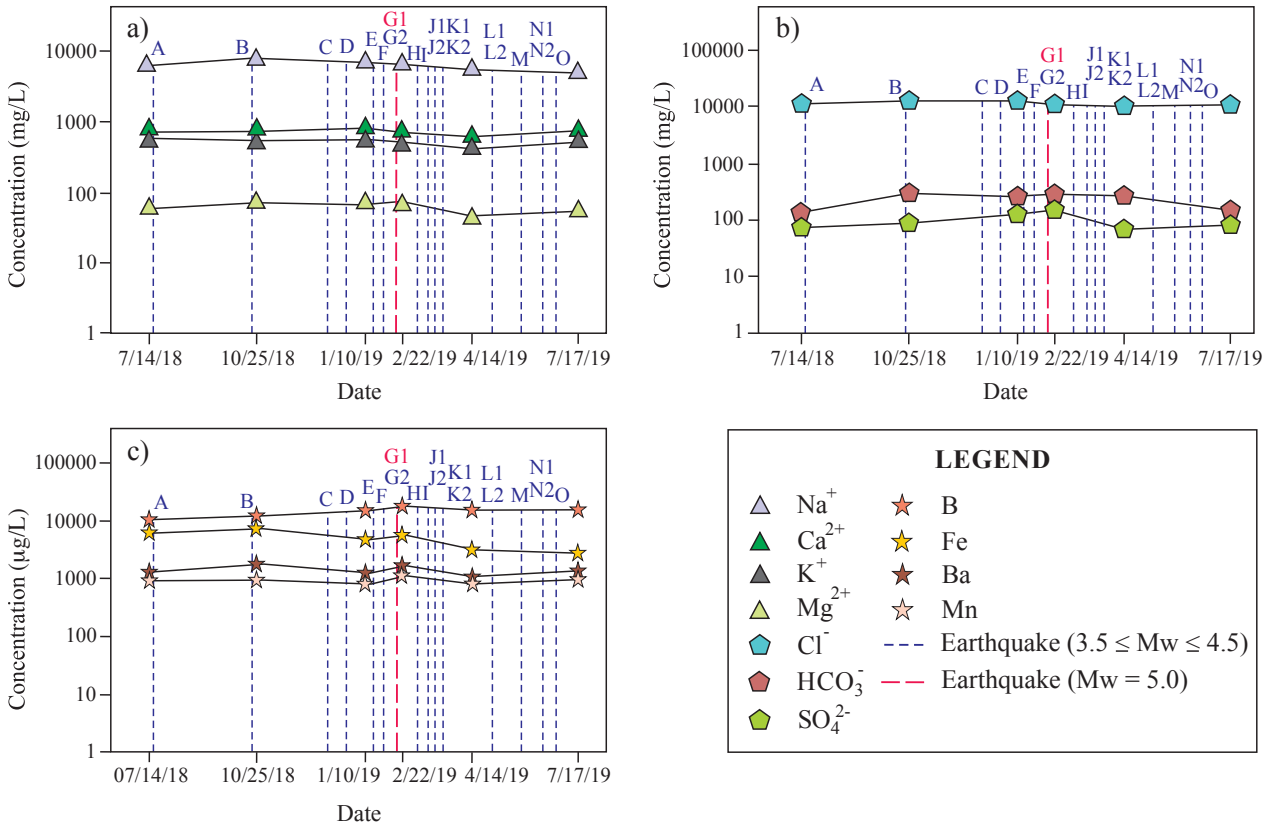

Figure 9. Temporal variations of a) cation, b) anion, and c) element concentrations in Kestanbol geothermal water connected with seismicity.

Mutzenberg (1997) identified the $\delta^{18}O$ value of K1 as –5.09‰ in March 1988, while the $\delta^{18}O$ value was identified as –5.41‰ in April 2019 in this study. In the last 31 years, the $\delta^{18}O$ value in the geothermal water was identified to reduce by 0.32‰. The increasing water-rock interaction at high temperatures over time is expected to increase the $\delta^{18}O$ content of geothermal water. The reduction in $\delta^{18}O$ values linked to time is thought to be the result of groundwater with shallow origin mixing with geothermal water through the fault and fracture zones related to regional seismic activity. Furthermore, the decrease in temperature of geothermal water after the Tartışık-Ayvacık earthquake probably confirms this interpretation. Long-term, regular, and more frequent monitoring of the $\delta^{18}O$, $\delta^{2}H$ and ^{3}H contents, in addition to identifying the chemical characteristics of geothermal waters, will lead to a better understanding of their relationship to seismic activities in the Kestanbol geothermal field.

4. Conclusion

Three principal processes determine the hydrogeochemical and isotopic characterization of the Kestanbol geothermal waters: meteoric water-fossil seawater mixing, prolonged water-rock interaction, and active tectonic. The Kaplıca fault extends NE–SW direction consistently and deeply and mainly controls the tectonic evolution and geothermal water movement in the Kestanbol geothermal field. Meteoric water undergoes deep circulation and is heated by the Kestanbol Pluton and high geothermal gradient and interacts with the reservoir rocks at higher temperatures mixing with deep-seated hot fossil seawater before rising along the permeable Kaplıca fault and fracture zones and emerging in the form of Kestanbol geothermal water.

The maximum discharge temperature of the geothermal well was measured as 74.6 °C; however, the reservoir temperature was about 120 °C calculated with the chalcedony geothermometer. A detailed geophysical survey is required to develop the geothermal energy potential of Kestanbol geothermal field, and new drillings must be performed to increase the flow rate and temperature of water. Furthermore, new drillings will provide detailed information about the hydrogeological conditions at depth. Due to the significant development of geothermal energy in the last decades, new utilization possibilities for Kestanbol geothermal waters must be evaluated.

The monitoring studies covering a total of six sampling periods over one year revealed temporal variations in physicochemical parameters and chemical composition of the geothermal waters related to seismic activity. It is recommended that long-term monitoring of chemical and isotopic composition of geothermal waters with more frequent sampling intervals be completed in future studies to determine the effect of seismic activities on the chemical and isotopic variations in Kestanbol geothermal waters. The variations in chemical composition of geothermal waters may be considered to be one of the probable precursor parameters to forecast impending earthquakes in this region.

Acknowledgment
The authors would like to thank the Scientific Research Projects Coordination Unit of Çanakkale Onsekiz Mart University for providing financial support for the projects with numbers FYL-2018-2709 and FHD-2019-2877. The authors would also like to thank to the three anonymous reviewers for their constructive comments that helped to improve the manuscript.

References

Akal C (2013). Coeval shoshonitic-ultrapotassic dyke emplacements within the Kestanbol Pluton, Ezine-Biga Peninsula (NW Anatolia). Turkish Journal of Earth Sciences 22 (2): 220-238. doi: 10.3906/yer-1202-1

Altunkaynak S, Dilek Y, Genc CS, Sunal G, Gertisser R et al. (2012). Spatial, temporal and geochemical evolution of Oligo–Miocene granitoid magmatism in western Anatolia, Turkey. Gondwana Resarch 21 (4): 961-986. doi: 10.1016/j.gr.2011.10.010

Ambraseys NN (1988). Engineering seismology: Part I. Earthquake Engineering and Structural Dynamics 17: 1-105. doi: 10.1002/eqe.4290170101

Arik F, Aydin U (2011). Mineralogical and petrographical characteristics of the Aladag skarn deposit (Ezine/Çanakkale-West Turkey). Scientific Research and Essays 6 (3): 592-606. doi: 10.5897/SRE10.853

Arnórsson S, Gunnlaugsson E, Svavarsson H (1983). The chemistry of geothermal waters in Iceland. III. chemical geothermometry in geothermal investigations. Geochimica et Cosmochimica Acta 47 (3): 567-577. doi: 10.1016/0016-7037(83)90278-8

Ates O, Tutkun SZ (2014). Hydrochemical changes in geothermal systems with Simav (Kutahya) earthquakes. Geological Bulletin of Turkey 57 (3): 25-40. doi: 10.25288/tjb.298711

Baba A, Ertekin C (2007). Determination of the source and age of the geothermal fluid and its effects on groundwater resources in Kestanbol (Canakkale-Turkey). In: 6th International Groundwater Quality Conference; Fremantle, Australia. pp. 148-155.

Balderer W, Leuenberger F, Suner F, Yalcin T, Stichler W (2002). Effects of the Cinarcik-Izmit August 17, 1999 earthquake on the composition of thermal and mineral waters as revealed by chemical and isotope investigations. Geofísica Internacional 41 (4): 385-391.

Barbier E, Fanelli M, Gonfiantini R (1983). Isotopes in geothermal energy exploration. International Atomic Energy Agency Bulletin 25 (2): 31-36.

Barka A, Kadinsky-Cade K (1988). Strike-slip fault geometry in Turkey and its influence on earthquake activity. Tectonics 7 (3): 663-684. doi: 10.1029/TC007i003p00663

Barka A (1992). The North Anatolian Fault Zone. Annales Tectonicae 6: 164-195.

Barka A (1997). Neotectonics of the Marmara region. In: Schindler C, Pfister M (editors). Active Tectonics of Northwestern Anatolia-The Marmara Poly-Project. VDF Hochschul Verlag AG an der ETH Zurich, pp. 55-87.

Beccaletto L (2003). Geology, correlations, and geodynamic evolution of the Biga Peninsula (NW Turkey). PhD, University of Lausanne, Lausanne-Switzerland.

Beccaletto L, Jenny C (2004). Geology and correlation of the Ezine zone: a Rhodope fragment in NW Turkey. Turkish Journal of Earth Sciences 13 (2): 145-176.

Bekler T, Demirci A (2018). Preliminary observations and assessment of Canakkale-Ayvacik earthquake activity. Journal of Advanced Research in Natural and Applied Sciences 4 (1): 1-13. doi: 10.28979/comufbed.393122

Belhai M, Fujimitsu Y, Bouchareb-Haouchine FZ, Haouchine A, Nishijima J (2016). A hydrochemical study of the Hammam Righa geothermal waters in north-central Algeria. Acta Geochimica 35 (3): 271-287. doi: 10.1007/s11631-016-0092-8

Belin B, Yalcin T, Suner F, Bozkurtoglu E, Gelir A et al. (2002). Earthquake-related chemical and radioactivity changes of thermal water in Kuzuluk-Adapazari, Turkey. Journal of Environmental Radioactivity 63 (3): 239-249. doi: 10.1016/S0265-931X(02)00031-0

Birkle P, Satir M (1992). Petrology, geochemistry and geochronology of a quartz-monzonite intrusion (Kestanbol granite) and their host rocks near Ezine, Biga-peninsula, NW Anatolia, Turkey. In: International Symposium on the Geology of the Black Sea Region; Ankara, Turkey. pp. 44-45.

Birkle P, Satir M (1995). Dating, geochemistry and geodynamic significance of the tertiary magmatism of the Biga Peninsula, NW Turkey. In: Erler A, Ercan T, Bingol E, Orcen S (editors). The geology of the Black Sea region, Ankara, Turkey: Directorate of Mineral Research and Exploration, pp. 171-180.

Caglar I, Demirorer M (1999). Geothermal exploration using geoelectric methods in Kestanbol, Turkey. Geothermics 28 (6): 803-816. doi: 10.1016/S0375-6505(99)00044-9

Cam D, Bulbul E, Kilinc O, San O (2013). Jeotermal akışkanların köken ilişkisi: Tuzla ve Babadere (Çanakkale) sahaları örneği. Maden Tetkik ve Arama Genel Müdürlüğü Doğal Kaynaklar ve Ekonomi Bülteni 15: 79-87 (in Turkish).

Chen Z, Du J, Zhou X, Li Y, Liu L et al. (2014). Hydrochemistry of the hot springs in western Sichuan Province related to the Wenchuan *Ms* 8.0 earthquake. Scientific World Journal 1-13. doi: 10.1155/2014/901432

Claesson L, Skelton A, Graham C, Dietl C, Mörth M et al. (2004). Hydrogeochemical changes before and after a major earthquake. Geology 32 (8): 641-644. doi: 10.1130/G20542.1

Clark ID, Fritz P (1997). Environmental Isotopes in Hydrogeology. 1st ed. New York, USA: Lewis Publishers.

Craig H (1961). Isotopic variations in meteoric waters. Science 133 (3465): 1702-1703. doi: 10.1126/science.133.3465.1702

Davalos-Elizondo E, Atekwana EA, Atekwana EA, Tsokonombwe G, Lao-Davila DA (2021). Medium to low enthalpy geothermal reservoirs estimated from geothermometry and mixing models of hot springs along the Malawi Rift Zone. Geothermics 89: 101963. doi: 10.1016/j.geothermics.2020.101963

Demirsoy N, Basaran CH, Sandalci S (2017). Kestampolis Kaplıcaları. 1st ed. Istanbul Turkey: Nobel Tıp Kitapevi (in Turkish).

Demirsoy N, Basaran CH, Sandalci S (2018). Historical Kestanbol hot springs: The water that resurrects. Lokman Hekim Journal 8 (1): 23-32.

Dewey JF, Sengor AMC (1979). Aegean and surrounding regions: complex multiplate and continuum tectonics in a convergent zone. Geological Society of America Bulletin 90 (1): 84-92. doi: 10.1130/0016-7606

Dilaver AT, Aydin B, Ozyurt NN, Bayari CS (2018). Türkiye yağışlarının izotop içerikleri (2012-2016). Devlet Su İşleri Genel Müdürlüğü ve Meteoroloji Genel Müdürlüğü Raporu. Ankara, Turkey (in Turkish).

Dotsika E (1991). Utilisation du geothermometre isotopique sulfate-eau en milieux de haute temperature sous influence marine potentielle: les systemes geothermaux de Grece. PhD, Paris-Sud University, Paris, France (in French with English abstract).

Du J, Amita K, Ohsawa S, Zhang Y, Kang C et al. (2010). Experimental evidence on formation of imminent and short-term hydrochemical precursors for earthquakes. Applied Geochemistry 25 (4): 586-592. doi: 10.1016/j.apgeochem.2010.01.015

Duru M, Pehlivan S, Aral IO, Senturk Y, Yavas F et al. (2012). Biga Yarımadası'nın Tersiyer öncesi jeolojisi. Yuzer E, Tunay G (editorler). Biga Yarımadası'nın Genel ve Ekonomik Jeolojisi. Ankara, Türkiye: Maden Tetkik ve Arama Genel Müdürlüğü Özel Yayın Serisi, s. 7-74 (in Turkish).

Eisenlohr T (1997). The thermal springs of the Armutlu Peninsula (NW Turkey) and their relationship to geology and tectonic. In: Schindler C, Pfister M (editors). Active Tectonics of Northwestern Anatolia-The Marmara Poly-Project. VDF Hochschul Verlag AG an der ETH Zurich, pp. 197-228.

Emre O, Dogan A, Yildirim C (2012). Biga Yarımadası'nın diri fayları ve deprem potansiyeli. Yuzer E, Tunay G (editorler). Biga Yarımadası'nın Genel ve Ekonomik Jeolojisi. Ankara, Türkiye: Maden Tetkik ve Arama Genel Müdürlüğü Özel Yayın Serisi, s. 163-198 (in Turkish).

Fytikas M, Giuliani O, Innocenti F, Marinelli G, Mazzuoli R (1976). Geochronological data on recent magmatism of Aegean Sea. Tectonophysics 31(1-2): 29-34. doi: 10.1016/0040-1951(76)90161-X

Fytikas M, Innocenti F, Manetti P, Peccerillo A, Mazzuoli R et al. (1984). Tertiary to Quaternary evolution of volcanism in the Aegean region. Geological Society of London Special Publications 17: 687-699. doi: 10.1144/GSL.SP.1984.017.01.55

Freeman JT (2007). The use of bromide and chloride mass ratios to differentiate salt-dissolution and formation brines in shallow groundwaters of the Western Canadian Sedimentary Basin. Hydrogeology Journal 15: 1377-1385. doi: 10.1007/s10040-007-0201-1

Fouillac C, Michard G (1981). Sodium/lithium ratio in water applied to geothermometry of geothermal reservoirs. Geothermics 10 (1): 55-70. doi: 10.1016/0375-6505(81)90025-0

Fournier RO, Truesdell AH (1973). An empirical Na-K-Ca geothermometer for natural waters. Geochimica et Cosmochimica Acta 37 (5): 1255-1275. doi: 10.1016/0016-7037(73)90060-4

Fournier RO (1977). Chemical geothermometers and mixing models for geothermal systems. Geothermics 5 (1-4): 41-50. doi: 10.1016/0375-6505(77)90007-4

Fournier RO (1979). A revised equation for the Na-K geothermometer. Transactions of the Geothermal Resources Council 3: 221-224.

Fournier RO, Potter RW (1982). A revised and expanded silica (quartz) geothermometer. Geothermal Resources Council Bulletin 11: 3-12.

Giggenbach WF (1988). Geothermal solute equilibria: derivation of Na-K-Mg-Ca geoindicators. Geochimica Cosmochimimica Acta 52 (12): 2749-2765. doi: 10.1016/0016-7037(88)90143-3

Goldberg ED, Broecker WS, Gross MG, Turekian KK (1971). Marine chemistry. In: Radioactivity in the Marine Environment. 1st ed. Washington, USA: The National Academies Press, pp. 137-146.

Gurer OF, Kaymakci N, Cakir S, Ozburan M (2003). Neotectonics of the southeast Marmara region, NW Anatolia, Turkey. Journal of Asian Earth Sciences 21 (9): 1041-1051. doi: 10.1016/S1367-9120(02)00140-2

Hartleb RD, Dolan JF, Kozacı O, Akyuz HS, Seitz GG (2006). A 2500-yr-long paleoseismologic record of large, infrequent earthquakes on the North Anatolian fault at Cukurcimen, Turkey. Geological Society of America Bulletin 118 (7-8): 823-840. doi: 10.1130/B25838.1

Herece E (1990). The fault trace of 1953 Yenice-Gonen earthquake and the westernmost known extension of the NAFZ in the Biga Peninsula. Bulletin of the Mineral Research and Exploration 111: 31-42.

Hsu H, Yeh H (2020). Factors controlling of thermal water hydrogeochemical characteristics in Tatun Volcano Group, Taiwan. Water 12 (9): 2473. doi: 10.3390/w12092473

Huang F, Jian C, Tang Y, Xu G, Deng Z et al (2004). Response changes of some wells in the mainland subsurface fluid monitoring network of China, due to the September 21, 1999, Ms 7.6 Chi-Chi Earthquake. Tectonophysics 390: 217-234. doi: 10.1016/j.tecto.2004.03.022

International Association of Hydrogeologists (IAH) (1979). Map of mineral and thermal water of Europe, Scale 1:500.000, International Association of Hydrogeologists, United Kingdom.

Ikeda Y, Suzuki Y, Herece E, Saroglu F, Isikara AM et al. (1991). Geological evidence for the last two faulting events on the North Anatolian Fault Zone in the Mudurnu valley, western Turkey. Tectonophysics 193 (4): 335-345. doi: 10.1016/0040-1951(91)90342-P

Italiano F, Bonfanti P, Pizzino L, Quattrocchi F (2010). Geochemistry of fluids discharged over the seismic area of the southern Apennines (Calabria region, southern Italy): implications for fluid-fault relationships. Applied Geochemistry 25 (4): 540-554. doi: 10.1016/j.apgeochem.2010.01.011

Kacar B, Ozden S, Ates O (2017). Geology and hydrogeochemistry of Gure (Balikesir) geothermal field and its relationship with active tectonic. Geological Bulletin of Turkey 60 (2): 243-258. doi: 10.25288/tjb.302968

Karaca Z, Sanliyuksel Yucel D, Yucel MA, Kamaci C, Cetiner Z et al. (2013). Çanakkale ili (Biga Yarımadası) jeotermal kaynakları ve özelliklerinin belirlenmesi, Biga Yarımadası jeotermal bilgi sistemi. Güney Marmara Kalkınma Ajansı DFD12/0011 No'lu Proje Raporu (in Turkish).

Karacik Z (1995). Relationship between young volcanism and plutonism in Ezine-Ayvacik (Canakkale) region. PhD, Istanbul Technical University, Istanbul, Turkey (in Turkish).

Karacik Z, Yilmaz Y (1995). Geology of the ignimbrite eruptions of Ezine-Ayvacik region, NW Anatolia. In: International Earth Science Colloquium on the Aegean Region; Izmir, Turkey. pp. 415-427.

Karacik Z, Yilmaz Y (1998). Geology of the ignimbrites and the associated volcano–plutonic complex of the Ezine area, northwestern Anatolia. Journal of Volcanology and Geothermal Research 85 (1): 251-264. doi: 10.1016/S0377-0273(98)00058-4

Karingithi CW (2009). Chemical geothermometers for geothermal exploration. In: Short Course IV on Exploration for Geothermal Resources; Lake Naivasha, Kenya. pp. 1-12.

Ketin I (1948). Uber die tektonisch-mechanischen Folgerungen aus den grossen Anatolischen Erdbeben des letzten Dezenniums. Geologische Rundschau 36: 77-83. doi: 10.1007/BF01791916

Ketin I, Roesli F (1953). Makroseismische untersuchungen über das nordwest Anatolische beben vom 18. März 1953. Eclogae Geologicae Helvetiae 46: 187-208.

King CY, Manga M (2018). Hydrological, Geochemical and Geophysical Changes Related to Earthquakes and Slow-Slip Events: Introduction. Pure and Applied Geophysics 175: 2407-2409. doi: 10.1007/s00024-018-1923-9

Kocyigit A (1988). Tectonic setting of the Geyve basin: age and total offset of the Geyve fault zone, East Marmara, Turkey. Journal of Pure and Applied Sciences 21: 81-104.

Kralik M (2015). How to estimate mean residence times of groundwater. Procedia Earth and Planetary Science 13: 301-306. doi: 10.1016/j.proeps.2015.07.070

Krauskopf KB, Bird DK (1995). Introduction to Geochemistry. 3rd ed. New York: McGraw-Hill.

Kavouridis T, Kuris D, Leonis C, Liberopoulou V, Leontiadis J et al. (1999). Isotope and chemical studies for a geothermal assessment of the island of Nisyros (Greece). Geothermics 28 (2): 219-239. doi: 10.1016/S0375-6505(99)00005-X

Kurcer A, Chatzipetros A, Tutkun SZ, Pavlides S, Ates O et al. (2008). The Yenice-Gonen active fault (NW Turkey): Active tectonics and palaeoseismology. Tectonophysics 453 (1-4): 263-275 doi: 10.1016/j.tecto.2007.07.010

Leaf W (1923). Strabo on the Troad. 1st ed. Cambridge, United Kingdom: Cambridge University Press.

Livaoglu R, Timuragaoglu MO, Serhatoglu C, Doven MS (2018). Damage during the 6-24 February 2017 Ayvacik (Canakkale) earthquake swarm. Natural Hazards and Earth System 18 (3): 921-934. doi: 0.5194/nhess-18-921-2018

Lucas LL, Unterweger MP (2000). Comprehensive review and critical evaluation of the half-life of tritium. Journal of Research of the National Institute of Standards and Technology 105 (4): 541-549. doi: 10.6028/jres.105.043

Lund JW, Toth AN (2021). Direct utilization of geothermal energy 2020 worldwide review. Geothermics 90: 101915. doi: 10.1016/j.geothermics.2020.101915

Mao X, Wang Y, Zhan H, Feng L (2015). Geochemical and isotopic characteristics of geothermal springs hosted by deep-seated faults in Dongguan Basin, Southern China. Journal of Geochemical Exploration 158: 112-121. doi: 10.1016/j.gexplo.2015.07.008

Marmara H, Sanliyuksel Yucel D, Ozden S, Yucel, MA (2020). Hydrochemistry and Environmental Impacts of Kestanbol Geothermal Fluid. Geological Bulletin of Turkey 63 (1): 97-116. doi: 10.25288/tjb.604842

McKenzie D (1972). Active tectonics of the Mediterranean region. Geophysical Journal of the Royal Astronomical Society 30: 109-185. doi: 10.1111/j.1365-246X.1972.tb02351.x

Mertoglu O, Simsek S, Basarir N (2020). Geothermal energy use: projections and country update for Turkey, In: World Geothermal Congress; Reykjavik, Iceland. pp. 1-11.

Michel RL (2005). Tritium in the hydrologic cycle. In: Aggarwal PK, Gat JR and Froehlich KFO (editors). Isotopes in the Water Cycle. 1st ed. Netherlands: Springer, pp. 53-66.

Mutlu H, Gulec N (1998). Hydrogeochemical outline of thermal waters and geothermometry applications in Anatolia (Turkey). Journal of Volcanology and Geothermal Research 85 (1-4): 495-515. doi: 10.1016/S0377-0273(98)00068-7

Mutzenberg S (1997). Nature and origin of the thermal springs in the Tuzla area, Western Anatolia, Turkey. In: Schindler C, Pfister M (editors). Active Tectonics of Northwestern Anatolia-The Marmara Poly-Project. VDF Hochschul Verlag AG an der ETH Zurich, pp. 301-320.

Nakagawa K, Yu Z, Berndtsson R, Hosonod T (2020). Temporal characteristics of groundwater chemistry affected by the 2016 Kumamoto earthquake using self-organizing maps. Journal of Hydrology 582: 124519. doi: 10.1016/j.jhydrol.2019.124519

Olmez E (1976). Çanakkale-Ezine Kestanbol sıcak su 1. sondajı kuyu bitirme raporu. Maden Tetkik ve Arama Genel Müdürlüğü Teknik Raporu, Ankara (in Turkish).

Ozden S, Over S, Poyraz SA, Gunes Y, Pinar A (2018). Tectonic implications of the 2017 Ayvacik (Canakkale) earthquakes, Biga Peninsula, NW Turkey. Journal of Asian Earth Sciences 154: 125-141. doi: 10.1016/j.jseaes.2017.12.021

Papadimitriou P, Kassaras I, Kaviris G, Tselentis GA, Voulgaris N et al. (2018). The 12th June 2017 Mw=6.3 Lesvos earthquake from detailed seismological observations. Journal of Geodynamics 115: 23-42. doi: 10.1016/j.jog.2018.01.009

Papazachos BC, Papazachou CB (1997). The earthquakes of Greece. 1st ed. Thessaloniki, Greece: Ziti Publications.

Pinar N (1953). Preliminary note on the earthquake of Yenice-Gönen, Turkey, March 18, 1953. Bulletin of the Seismological Society of America 43 (4): 307-310.

Piper AM (1944). A graphic procedure in the geochemical interpretation of water analyses. Transactions American Geophysical Union 25 (6): 914-928. doi: 10.1029/TR025i006p00914

Ravikumar P, Somashekar RK (2011). Environmental tritium (^{3}H) and hydrochemical investigations to evaluate groundwater in Varahi and Markandeya river basins, Karnataka, India. Journal of Environmental Radioactivity 102 (2): 153-162. doi: 10.1016/j.jenvrad.2010.11.006

Rockwell T, Barka A, Dawson T, Akyuz S, Thorup K (2001). Paleoseismology of the Gazikoy-Saros segment of the North Anatolia fault, northwestern Turkey: Comparison of the historical and paleoseismic records, implications of regional seismic hazard, and models of earthquake recurrence. Journal of Seismology 5: 433-448. doi: 10.1023/A:1011435927983

Roumelioti Z, Kiratzi A (2010). Incorporating different source rupture characteristics into simulations of strong ground motion from the 1867, M7.0 earthquake on the island of Lesvos (NE Aegean Sea, Greece). Bulletin of the Geological Society of Greece 43 (4): 2135-2143. doi:https://doi.org/10.12681/bgsg.11404

Sahin SY, Orgun Y, Gungor Y, Goker AF, Gultekin AH et al. (2010). Mineral and whole-rock geochemistry of the Kestanbol Granitoid (Ezine-Canakkale) and its mafic microgranular enclaves in Northwestern Anatolia: Evidence of felsic and mafic magma interaction. Turkish Journal of Earth Sciences 19: 101-122. doi: 10.3906/yer-0809-3

Samilgil E (1966). Çanakkale'nin Tuzla ve Kestanbol sıcak su havzalarında jeotermal enerji araştırması yönünden hidrojeolojik etüdü. Maden Tetkik ve Arama Genel Müdürlüğü Teknik Raporu, Ankara (in Turkish).

Sanliyuksel D, Baba A (2011). Hydrogeochemical and isotopic composition of a low-temperature geothermal source in Northwest Turkey: Case sudy of Kirkgecit geothermal area. Environmental Earth Sciences 62 (3): 529-540. doi: 10.1007/s12665-010-0545-z

Sanliyuksel Yucel D, Balci N, Baba A (2016). Generation of acid mine lakes associated with abandoned coal mines in Northwest Turkey. Archives of Environmental Contamination and Toxicology 70 (4): 757-782. doi: 10.1007/s00244-016-0270-z

Schoeller H (1955). Geochimie des eaux souterraines aux eaux de gisements de petrole. Revue de l'Institut Français du Pétrole et annales des combustibles liquides 10: 219-246.

Sengor AMC, Gorur N, Saroglu F (1985). Strike-slip faulting and related basin formation in zones of tectonic escape: Turkey as a case study. In: Biddle KT, Christie-Blick N (editors), Strike-slip Deformation, Basin Formation and Sedimentation. Oklahoma, USA: Society of Economic Mineralogist and Paleontologists Special Publication, pp. 227-264.

Seyitoglu G, Kaypak B, Aktug B, Gurbuz E, Esat K et al. (2016). A hypothesis for the alternative southern branch of the North Anatolian Fault Zone, Northwest Turkey. Geological Bulletin of Turkey 59(2): 115-130. doi: 10.25288/tjb.298155

Shi Z, Wang G, Manga M, Wang C (2015). Mechanism of co-seismic water level change following four great earthquakes–insights from co-seismic responses throughout the Chinese mainland. Earth and Planetary Science Letters 430: 66-74. doi: 10.1016/j.epsl.2015.08.012

Simsek S, Yildirim N (2000). Geothermal activity at 17 August on 12 November 1999 eastern Marmara earthquake region, Turkey. In: International Geothermal Association Meeting; Antalya, Turkey. pp. 1-9.

Siyako M, Burkan KA, Okay AI (1989). Tertairy geology and hydrocarbon potential of the Biga and Gelibolu Peninsulas. Turkish Association of Petroleum Geologists 1 (3): 183-199 (in Turkish).

Skelton A, Claesson L, Chakrapani G, Mahanta C, Routh J et al. (2008). Coupling between seismic activity and hydrogeochemistry at the Shillong Plateau, Northeastern India. Pure and Applied Geophysics 165: 45-61. doi: 10.1007/s00024-007-0288-2

Song SR, Chen YL, Liu CM, Ku WY, Chen HF et al. (2005). Hydrochemical changes in spring waters in Taiwan: implications for evaluating sites for earthquake precursory monitoring. TAO 16 (4): 745-762. doi:10.3319/TAO.2005.16.4.745

Soysal H, Sipahioglu S, Kolcak D, Altinok Y (1981). Türkiye ve çevresinin tarihsel deprem kataloğu. Türkiye Bilimsel ve Teknolojik Araştırma Kurumu TBAG 341 No'lu Proje Raporu (in Turkish).

Sozbilir H, Ozkaymak C, Uzel B, Sumer O, Eski S et al. (2016). Paleoseismology of the Havran-Balıkesir Fault Zone: evidence for past earthquakes in the strike-slip dominated contractional deformation along the southern branches of the North Anatolian Fault in northwest Turkey. Geodinamica Acta 28 (4): 254-272. doi: 10.1080/09853111.2016.1171111

Sozbilir H, Uzel B, Sumer O, Eski S, Softa M et al. (2018). Seismic sources of (14th January-20th March 2017) Canakkale-Ayvacik earthquake swarm. Eskisehir Technical University Journal of Science and Technology B- Theoritical Sciences 6: 1-17. (in Turkish). doi: 10.20290/aubtdb.498805

Suer S, Gulec N, Mutlu H, Hilton DR, Cifter C et al. (2008). Geochemical monitoring of geothermal waters (2002–2004) along the North Anatolian Fault Zone, Turkey: spatial and temporal variations and relationship to seismic activity. Pure and Applied Geophysics 165: 17-43. doi: 10.1007/s00024-007-0294-4

Tasci MA (1995). Hellenistic pottery of Troad in Canakkale museum. MSc, Ataturk University, Erzurum, Turkey (in Turkish).

Taymaz T, Jackson J, McKenzie D (1991). Active tectonics of the north and central Aegean Sea. Geophysical Journal International 106 (2): 433-490. doi: 10.1111/j.1365-246X.1991.tb03906.x

Temizel EH, Gultekin F (2018). Hydrochemical, isotopic, and reservoir characterization of the Pasinler (Erzurum) geothermal field, eastern Turkey. Arabian Journal of Geosciences 11: 3. doi: 10.1007/s12517-017-3349-6

TS266 (2005). Regulation on water intended for human consumption in Turkey. Turkish Standards Institute, Ankara (in Turkish).

Tokcaer M (2007). Geochemical cycle of boron and isotope fractionation in geothermal fluids of western Anatolia. PhD, Dokuz Eylul University, Izmir, Turkey (in Turkish).

Tsunogai U, Wakita H (1996). Anomalous changes in groundwater chemistry possible precursors of the 1995 Hyogoken Nanbu Earthquake, Japan. Journal of Physics of the Earth 44: 381-390. doi: 10.4294/jpe1952.44.381

Vengosh A, Helvaci C, Karamanderesi IH (2002). Geochemical constraints for the origin of thermal waters from western Turkey. Applied Geochemistry 17 (3): 163-183. doi: 10.1016/S0883-2927(01)00062-2

Verma MP (2000). Revised quartz solubility temperature dependence equation along the water-vapor saturation curve. In: World Geothermal Congress; Kyushu-Tohoku, Japan. pp. 1927-1932.

Yalcin T, Suner F, Balderer W, Bozkurtoglu E (2003). Effects of the 17 August, 1999 earthquake on the heavy metal composition of thermal waters in the Marmara Region, Northwest Turkey: Is it a precursor. Journal of the Geological Society of India 62 (5): 549-557.

Yalcin T (2007). Geochemical characterization of the Biga Peninsula thermal waters (NW Turkey). Aquatic Geochemistry 13: 75-93. doi: 10.1007/s10498-006-9008-2

Yalcin T, Sarp S (2012). Biga Yarımadası termal sularının jeokimyası ve jeotermal potansiyeli, In: Yuzer E, Tumay G (editorler). Biga Yarımadası'nın Genel ve Ekonomik Jeolojisi. Ankara, Türkiye: Maden Tetkik ve Arama Genel Müdürlüğü Özel Yayın Serisi, pp. 289-301 (in Turkish).

Yaltirak C (2002). Tectonic evolution of the Marmara Sea and its surroundings. Marine Geology 190 (1-2): 493-529. doi: 10.1016/S0025-3227(02)00360-2

Yuce G, Ugurluoglu DY, Adar N, Yalcin T, Yaltirak C et al. (2010). Monitoring of earthquake precursors by multi-parameter stations in Eskisehir region (Turkey). Applied Geochemistry 25 (4): 572-579. doi: 10.1016/j.apgeochem.2010.01.013